# Sustainable 3D Printed Electronics with Sheath Conductors

**by**

**Daina V. Baker**

B.Sc., Simon Fraser University, 2018

Thesis Submitted in Partial Fulfillment of the
Requirements for the Degree of
Master of Applied Science

in the
School of Sustainable Energy Engineering
Faculty of Applied Sciences

© Daina V. Baker 2021
SIMON FRASER UNIVERSITY
Spring 2021

Copyright in this work rests with the author. Please ensure that any reproduction or re-use is done in accordance with the relevant national copyright legislation.

## Declaration of Committee

| | |
|---|---|
| **Name:** | **Daina V. Baker** |
| **Degree:** | **Master of Applied Science** |
| **Thesis title:** | **Sustainable 3D Printed Electronics with Sheath Conductors** |
| **Committee:** | **Chair:** Manpreet Kaur<br>Lecturer, Sustainable Energy Engineering |
| | **Woo Soo Kim**<br>Supervisor<br>Associate Professor, Mechatronic Systems Engineering |
| | **Sami Khan**<br>Committee Member<br>Assistant Professor, Sustainable Energy Engineering |
| | **Michael Adachi**<br>Examiner<br>Assistant Professor, Engineering Science |

## Abstract

Sustainable manufacturing practices have been an essential consideration in recent years. 3D printing will be a key technology in the transition towards sustainability because it minimizes material consumption and waste generation. One area that could benefit from 3D printing techniques would be the production of printed circuit boards and electronics in which most of the copper used is etched in subsequent steps. Comparatively, 3D printing minimizes waste by depositing conductive material only where desired. However, the conductive material used, commonly a silver-based printable material, is expensive and further reductions are required to ensure sustainability. In high frequency applications, owing to the skin effect, the core of a conductor carries little electrical current and thus could be replaced with a cheaper plastic. To accomplish this, custom nozzles capable of printing these sheath conductors were developed and tested by printing an embedded inductor for wireless power transfer.



**Keywords**: Core-Shell; Coaxial 3D Printing; Sustainable Manufacturing; 3D Printed Electronics; Structural Electronics

## Dedication

To my parents and my friends, thank you for your constant support.

# Acknowledgements

First and foremost, I would like to acknowledge my senior supervisor Dr. Woo Soo Kim without which none of this would be possible. I have learned much about project planning, goal settings and the value of concrete milestones. For that I am grateful. Above all, I am thankful for his patience and guidance throughout this long process, and his constant words of encouragement in times where experiments were unfruitful. A tremendous thanks to him for his supervision.

I would like to further offer my earnest appreciation to my supervisory committee, Dr. Manpreet Kaur, Dr. Sami Khan, and Dr. Michael Adachi, for their valuable feedback and suggestions on my research project. I would also like to offer my thanks for the invaluable advice Mustafa Sajid from the School of Mechatronic Systems Engineering.

To the new friends I have made in the Additive Manufacturing Lab, I would like to thank each of you for the continued support throughout this process. Thank you, Tae-Ho, Xin, and Chao, for always being able to find the time for our quick discussions on research and on life.

To my new friends in the School of Sustainable Energy Engineering, I would like to thank you as well for the support and the thought-provoking discussions during our seminar sessions. Thank you to Vivian Neal as well, for arranging such an opportunity for the program, and for providing tutelage, guidance, and mentorship like none other.

Lastly, I would like to extend my utmost gratitude to my friends, Brahmjot, Rameez and Joanne, who have always been my support and anchor in my work and my studies. Thank you to each for lending an ear when times got dark and for sharing in my joy when times got bright.

# Table of Contents

Declaration of Committee ..... ii
Abstract ..... iii
Dedication ..... iv
Acknowledgements ..... v
Table of Contents ..... vi
List of Tables ..... viii
List of Figures ..... ix
List of Acronyms ..... xi
Executive Summary ..... xii

**Chapter 1. Introduction ..... 1**
1.1. Motivation & Objectives ..... 1
1.2. Thesis Overview ..... 2
1.3. Sustainability and 3D Printing ..... 2
1.3.1. The Skin Effect and its Origins ..... 4
1.3.2. Current Density Distribution – Solid Conductor vs Hollow ..... 5
1.4. Generating Core-Shell Structures and Coaxial 3D Printing ..... 7
1.4.1. Coaxial Nozzle ..... 8
1.4.2. Core-Shell Filament ..... 9
1.5. Structural & Embedded Electronics Systems, 3D Printing Electronics & Wireless Power Transfer ..... 11
1.5.1. Structural Electronics – Substrate ..... 13
1.5.2. Structural Electronics – Conductive Traces ..... 14
1.5.3. Inductors & Wireless Power Transfer ..... 16

**Chapter 2. Design of Core-shell Nozzles ..... 21**
2.1. Objective and Plan for Core-Shell Nozzle Design ..... 21
2.1.1. Skin Depth ..... 21
2.1.2. Machining and High-resolution 3D Printing ..... 22
2.2. Nozzle Prototypes ..... 22
2.2.1. Thermal Simulation ..... 23
2.2.2. Nozzle Prototype 1 ..... 24
2.2.3. Nozzle Prototype 2 ..... 25
2.2.4. Nozzle Prototype 3 ..... 25

**Chapter 3. 3D Printing with Core-Shell Nozzles ..... 27**
3.1. Sustainability in Sheath Conductors ..... 27
3.2. Printing Process ..... 28
3.2.1. Inductor Design ..... 29
3.2.2. Shell Material Selection and Preparation ..... 29
3.2.3. Core Material Selection ..... 30
3.2.4. Core Material Selection ..... 31
3.2.5. Magnetic Filament Preparation ..... 31

3.3. Core-Shell Inductors ..... 32
3.3.1. Preliminary Simulation of Core-Shell Inductors ..... 32
3.3.2. Simulation and Characterization of Core-Shell Inductors ..... 33

**Chapter 4. Demonstration of Wireless Power Transfer with 3D Printed Inductors ..... 36**
4.1. Experimental Setup ..... 36
4.2. Coupling Coefficient ..... 38
4.3. Maximum Power Transfer Efficiency ..... 39
4.4. Conclusions ..... 40

**Chapter 5. Conclusions and Future Work ..... 42**
5.1. Conclusions ..... 42
5.2. Future Work ..... 44

**References ..... 45**

# List of Tables

Table 1: Theoretical calculation of material savings for the core-shell printed inductors based on estimated values and designs. .....28

# List of Figures


Figure 1.1: Cost per part based on the complexity of the product. Reprinted with permission [9] Copyright © 2014 Elsevier B.V. All rights reserved. ..... 3

Figure 1.2: Visualization of Skin Depth for a solid conductor (top) and hollow conductor (bottom) at 1 Hz (left) and 1 MHz (right). ..... 6

Figure 1.3: Current density across the diameter of conductor for a solid conductor (top) and a hollow conductor (bottom). Frequencies of 1E0 Hz and 1E4 Hz are overlapping in the graph. Values between 1E2 and 1E3 were omitted as they would have overlapped as well. ..... 7

Figure 1.4: Coaxial nozzle for printing hollow alginate tubes. Reprinted with permission [19], Copyright © 2015 Elsevier Ltd. All rights reserved. ..... 8

Figure 1.5: The coaxial printing process requires balancing the surface tension (FT) and the drag force (Fd) (a + insert). If the surface tension is too high, droplets form (b). If viscous drag is correct, a smooth jet occurs (c). Reprinted with permission[23], Copyright © 2019 WILEY-VCH Verlag GmbH & Co. KGaA, Weinheim ..... 9

Figure 1.6: Preparation of core-shell filament for 3D printing. Reprinted with permission from [22], Copyright © 2019, American Chemical Society. ... 10

Figure 1.7: Careful control of the diffusion of silver in photocurable resin affects the distribution of silver in the final product.[24] Open access Copyright © 2021, Crown ..... 10

Figure 1.8: Comparison of conventional PCB manufacturing (A) and a 3D Printing approach to PCB manufacturing (B). Reprinted with permission[13], Copyright © 2018 Elsevier Inc. ..... 12

Figure 1.9: Selected examples of structural electronics. An electric egg timer (a) is shown with embedded components. Reprinted with permission [37], Copyright © 2019, IEEE. ..... 13

Figure 1.10: Overview of planar spiral inductor and major parameters. ..... 17

Figure 1.11: Categories of wireless power transfer. Reprinted with permission [61], Copyright © 2013, Springer Science Business Media New York ..... 18

Figure 1.12: Factors influencing coupling factor. Reproduced with permission[65] Copyright © 2021 Wireless Power Consortium, Inc. ..... 19

Figure 1.13: Magnetic field lines between two coupled coils without a backplane (left) and with a backplane (right). ..... 20

Figure 2.1: Thermal simulation (a,b) and actual nozzle of prototype 1 (c). The internal portion of the nozzle is shown in (a) and the front in (b). ..... 24

Figure 2.2: Thermal simulation (a,b) and actual nozzle of prototype 2 (c). The internal portion of the nozzle is shown in (a) and the front in (b). ..... 25

Figure 2.3: Core-shell filament (sheath conductor) generated by prototype 2. ..... 25

Figure 2.4: Thermal simulation (a,b) and actual nozzle of prototype 3 (c). The internal portion of the nozzle is shown in (a) and the front in (b). ..... 26

Figure 3.1: Core-shell 3D printer setup. ..... 28

Figure 3.2: CAD renderings of the three designs. Thickness has been exaggerated to emphasize the core. Single, double and triple widths (a,b,c respectively) are shown. ....29
Figure 3.3: Preparation of magnetic filament for core-shell 3D printing. The Filabot was used to extrude filament for printing. ....31
Figure 3.4: Simulated inductance of single, double, and triple width inductors with various core materials. ....33
Figure 3.5: Prints of the single, double, and triple width inductors on PCL substrate. ....34
Figure 3.6: CAD representation of single-width embedded inductors (a) and exploded view in (b). Printed samples with a backplane of PCL (c) and Ferrite-PCL (b). ....34
Figure 3.7: Simulated and experimental inductances for embedded single, double, and triple width inductors printed on PCL and Ferrite-PCL (Fer) backplanes. ....35
Figure 4.1: Measurement of coupling coefficient using an LCR meter. ....37
Figure 4.2: Simulated (a) and experimental (b) results for coupling coefficient of single, double, and triple width inductors and commercial inductor. ....38
Figure 4.3: Simulated (a) and experimental (b) results for the maximum power transfer efficiency single, double, and triple width inductors and commercial inductor. ....39
Figure 4.4: Quality factor (a) and resistance measurements for the single, double, and triple width inductor. ....40

# List of Acronyms

| | |
|---|---|
| AC | Alternating Current |
| AM | Additive Manufacturing |
| b.p. | Boiling Point |
| CAD | Computer Assisted Design |
| CFR | Carbon Fiber Reinforced |
| DC | Direct Current |
| DIW | Direct-ink Writing |
| DMF | *N*,*N*-dimethylformamide |
| EMF | Electromotive Force |
| FDM | Fused Deposition Modelling |
| Fer | Ferrite-PCL Composite |
| FFF | Fused Filament Fabrication |
| LAC | Library and Archives Canada |
| PCB | Printed Circuit Board |
| PCL | Polycaprolactone |
| PIPS | Polymer-induced Phase Separation |
| PLA | Polylactic acid |
| rpm | Revolutions Per Minute |
| SDG | Sustainable Development Goal |
| SFU | Simon Fraser University |
| SLA | Stereolithography |
| THF | Tetrahydrofuran |
| WPT | Wireless Power Transfer |

## Executive Summary

As the world shifts towards a model of greater sustainability, 3D printing presents itself as an essential technology in the transition. The ability for 3D printing techniques to prepare complex and fully customizable structures, while additionally reducing material consumption and waste generation, is unmatched by conventional processing techniques. The production of printed circuit boards and electronics has much to gain from the adoption of such techniques, especially because most of the copper deposited in the production of circuit boards is etched away. However, 3D printed techniques available for electronics are heavily reliant on silver-based conductive materials rendering them prohibitively expensive for wide adoption. Rather than changing the conductive material to carbon or copper, which, albeit cheaper, are highly resistive and difficult to work with respectively, it would be beneficial to reduce the amount of silver required. If the conductive material is limited only to the outer layer of a printed trace, the amount of silver could be reduced. To produce such a core-shell structure, a sheath conductor, a novel 3D printing nozzle has been designed and tested. Herein, the generation of inductors for wireless power transfer made from sheath conductor is described and detailed.

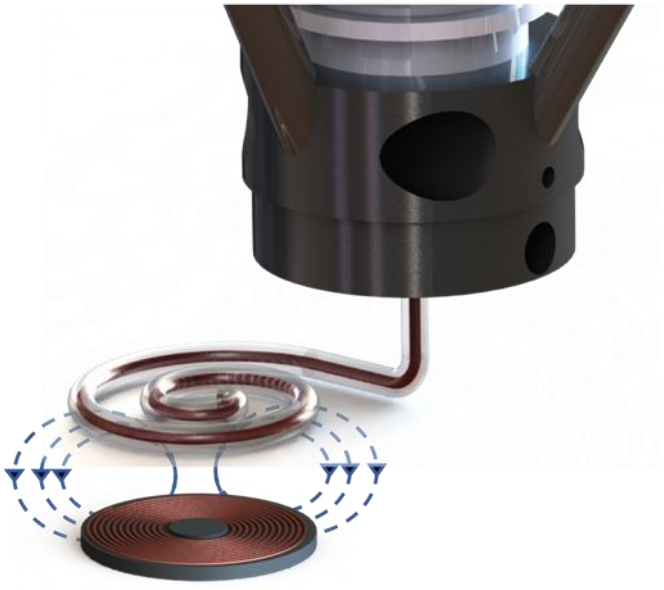

**Core-shell printing of inductors for wireless power transfer.**

# Chapter 1.

# Introduction

## 1.1. Motivation & Objectives

3D printing presents itself as a great opportunity for increasing sustainability in manufacturing. In many cases, the technique also allows for greater complexity and customizability than conventional manufacturing techniques which would be either too costly or infeasible to produce. In addition, because 3D printing techniques are additive, rather than subtractive, the material is deposited only where it is required, thus minimizing material consumption and waste generation. Consequently, compared with conventional circuit board manufacturing and electronic manufacturing, 3D-printed equivalents require less material and generate less waste. However, in many cases, materials with adequate conductivity for electronic applications require silver-based materials, which can be prohibitively expensive. Efforts to decrease the associated cost have been focused on substituting the silver for a less precious metal. However, the use of a less precious metal requires hazardous chemicals either during the processing or post-processing. Thus, silver remains the premier choice for conductive applications. An alternative would be to reduce the silver required to produce a conductive trace.

In high frequency alternating current (AC), current density is localized primarily to the surface of the conductor. This concentration of current results in a decreased current density in the core. At sufficiently high frequencies, (for example 1 GHz), the current is localized to just a few microns at the surface. Consequently, cables that carry high frequency current are either stranded (multiple insulated bundles of wire), to increase current carrying capacity, or hollow, to reduce costs and weight of the conductor. If a similar conductor structure could be 3D printed, it would likewise be possible to reduce the costs associated with conductive 3D printing. As it would be difficult to produce a fully hollow conductor with 3D printing, an alternative would be to substitute the core of a conductor with a much cheaper, inert material, generating a core-shell structure.

The objective of this thesis project is to produce nozzles capable of printing and generating conductive core-shell 3D filaments and to demonstrate this in structural electronics

applications. Wireless power transfer through inductive coupling was chosen as a demonstration because inductive coupling represents a use case of high frequency current that requires inductors with low resistance.

## 1.2. Thesis Overview

The thesis has been divided into five chapters. In chapter 1, concepts related to the research topic will be discussed and reviewed. The discussion will begin with sustainability, followed by an overview of structural electronics, a discussion of the skin effect and how it relates to core-shell printing. Finally, a discussion of inductors and inductive coupling will close the chapter. Chapter 2 will discuss the planning and designing process of the core-shell nozzles for printing. Chapter 3 will highlight the inductor design process, the relevant simulations, and the results of inductor printing. Chapter 4 will discuss the results of power transfer with the printed inductors. Finally, chapter 5 will summarize the thesis and provide direction for future work.

Overall, this work builds on the present literature to establish a novel method of coaxial printing. Previous approaches have focused primarily on the coextrusion of either two pastes, two thermoplastics, or a fibrous or liquid material surrounded by thermoplastic. This work instead presents an unexplored method of coating a thermoplastic with a conductive metal paste. In this way, sheath conductors can be printed to effect a reduction in material consumption for conductive printing, while also maintaining high conductivity and effectiveness.

## 1.3. Sustainability and 3D Printing

In 2015, the United Nations announced in their “2030 Agenda for Sustainable Development” 17 Sustainable Development Goals (SDGs)[1] which outline the steps required for the development of a global sustainable society. Together, the SDGs cover the three dimensions, or pillars, of sustainable development—economic, social, and environmental sustainability. One area that is under constant pressure to increase sustainability, would be in manufacturing.

Greater sustainability in manufacturing would address and result in improvements in economic, social, and environmental outcomes.[2] As part of the new industrial revolution,

3D printing, and more broadly Additive Manufacturing (AM), will be a key driver in increased sustainability.[3], [4] A 2014 study has predicted the potential impact of 3D printing on reducing manufacturing costs, energy consumption, and $CO_2$ emissions by $170-593 billion USD, 2.54-9.30 EJ, and 130.5-525.5 Mt, respectively, by 2025.[5] Beyond the advantages of allowing for cheap localized production, reducing shipping costs and expenditure, and closing the production cycle, 3D printing requires less material and energy.[5]–[8] There is minimal waste and energy during 3D printing manufacturing because 3D printing technologies selectively deposit material: it is an additive, rather than subtractive technique. Thus, it can be considered a more sustainable option in many regards.

Additionally, 3D printing can create complex and highly customized structures for “free” as the cost for manufacturing remains relatively constant (Figure 1.1).[9] Similar structures produced through traditional methods of manufacturing would be either impossible or prohibitively expensive to replicate. The increased complexity allowed by 3D printing can result in a further reduction in material consumption without compromising strength,[10] or unique structural properties such as the case with architectured and meta-materials where the properties of the printed structure are different than the bulk material.[11], [12] It is also possible to combine printing technologies to add additional complexity. With the advancement in multi-material 3D printing, the addition of printable conductive materials and pick-and-place machinery, the field of structural and embedded electronics is also accessible.

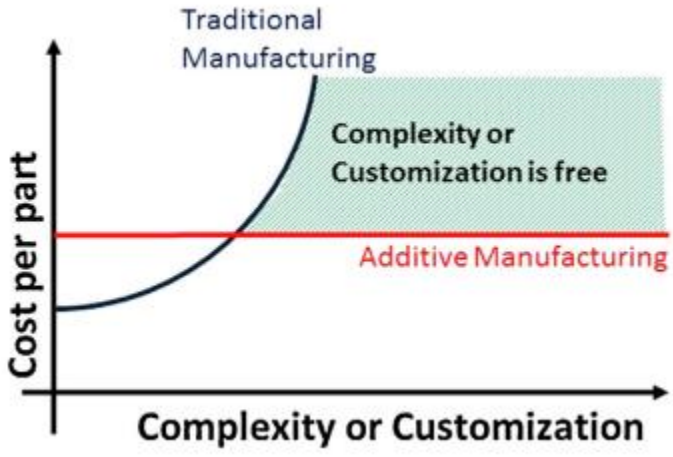


**Figure 1.1: Cost per part based on the complexity of the product. Reprinted with permission [9] Copyright © 2014 Elsevier B.V. All rights reserved.**

Overall, the potential of 3D printing technologies to move manufacturing in a more sustainable direction is immense, and one area that could benefit from greater sustainability would be electronics and printed circuit board manufacturing.[13] Because 3D printing is an additive technique, there is the potential to save a lot of material. However, in some cases, there could be an even greater saving. Because of the skin effect (section 1.3.1), the core of a conductor may not be carrying much or any current. Thus, using a core-shell structure (section 1.4) where only the shell is conductive would result in a better material economy in the production of 3D printed structural electronics (section 1.5).

### 1.3.1. The Skin Effect and its Origins

In high frequency alternating current (AC), there is a tendency for electric current density to concentrate at the surface of a conductor. Current density (J) in a conductor decays exponentially from its surface current density ($J_s$) in relation to depth (d) from the surface (equation 1.1).[14]–[16] The depth of penetration or skin depth (δ) is inversely related to the frequency (f), and the conductivity (σ) of the conductor (equation 1.2). Based on these two equations one can conclude that current density drops off exponentially from the surface at sufficiently high frequencies (> 1 MHz). Therefore, at high frequencies, little or no current density is present in the core of a conductor with a radius greater than the skin depth; consequently, little current is being carried in this region as current is the integral of current density across the cross-sectional area. This decrease results in higher effective resistance, and greater ohmic losses.

$$J = J_s e^{-d/\delta} \tag{1.1}$$

$$\delta = \frac{1}{\sqrt{\pi f \mu \sigma}} \tag{1.2}$$

The skin effect arises because of a consequence of induction. From the Maxwell-Faraday equation (equation 1.3), a time-varying magnetic field (**B**) always accompanies a time-varying electric field (**E**), and the converse is also true. In an AC circuit, the alternating current generates a time-varying magnetic field and this field, in turn, induces an alternating current in the conductor. By Lenz's law (equation 1.4), the induced electromotive force (EMF, $\mathcal{E}$) or back EMF, opposes the changing magnetic flux ($\Phi_b$) that

generated it. The induced EMF is greater at the center of the conductor than at the surface and is more pronounced at higher frequencies. Overall, these induced currents result in a decrease in current density at the center of the conductor, and thus a decrease in current being carried at the centre of the conductor.

$$\nabla \times \boldsymbol{E} = -\frac{\partial \boldsymbol{B}}{\partial \boldsymbol{t}} \tag{1.3}$$

$$\mathcal{E} = -\frac{\partial \Phi_B}{\partial t} \tag{1.4}$$

The unequal distribution of current results in increased effective resistance, thus greater ohmic losses. Strategies to minimize these losses have been explored and focus on optimizing the conductor diameter (or thickness) for the application frequency or using a hollow conductor. [16], [17]

### 1.3.2. Current Density Distribution – Solid Conductor vs Hollow

The simulated current density for a copper conductor (⌀ = 1.3 mm) at low frequency (1 Hz) is shown in Figure 1.2a. At such a low frequency, current density is uniformly distributed across the entire conductor. However, at higher frequency (1 MHz), current density is concentrated close to the surface (δ ≈ 65 μm, Figure 1.2b). A hollow conductor similarly has the same trend as a solid conductor. At low frequency, current density is uniformly distributed across the conductor (figure 1.2c). At high frequencies (1 MHz), current density is concentrated at the surface (figure 1.2d).

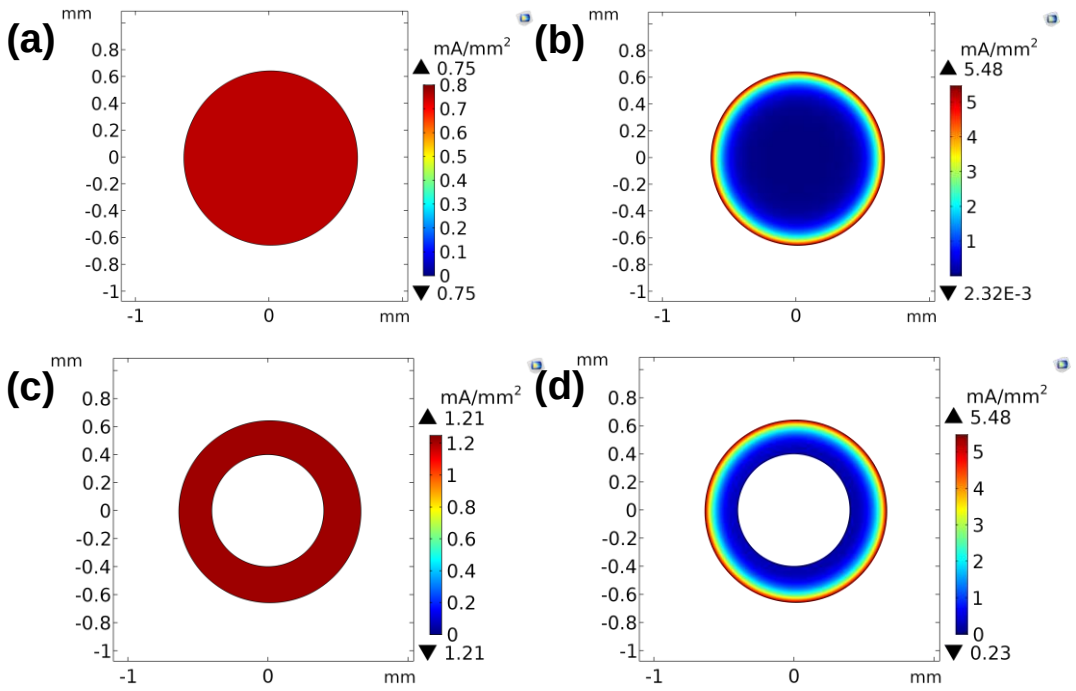


**Figure 1.2: Visualization of Skin Depth for a solid conductor (top) and hollow conductor (bottom) at 1 Hz (left) and 1 MHz (right).**

In both cases, as frequency increases, current density deeper in the conductor tends toward zero (figure 1.3). In this simulation, frequencies between 1E0 Hz and 1E4 Hz have near identical current density distributions and thus are overlapping in the graph. It is not until 1E5 Hz and 1E6 Hz that the skin effect becomes obvious at this scale. It can also be seen that removing a portion of the at the centre has had little to no effect on the overall distribution. As can be seen, using a hollow conductor or a core-shell structure where the core is replaced with a dielectric material, would have a minimal consequence on the performance of the conductor.

Because of the skin effect, solid conductors are not as efficient as hollow conductors in some applications. To reduce the consumption of conductive material in 3D printing, it would be best to adopt a core-shell structure, which is analogous to a hollow conductor, where only the shell is composed of conductive material.

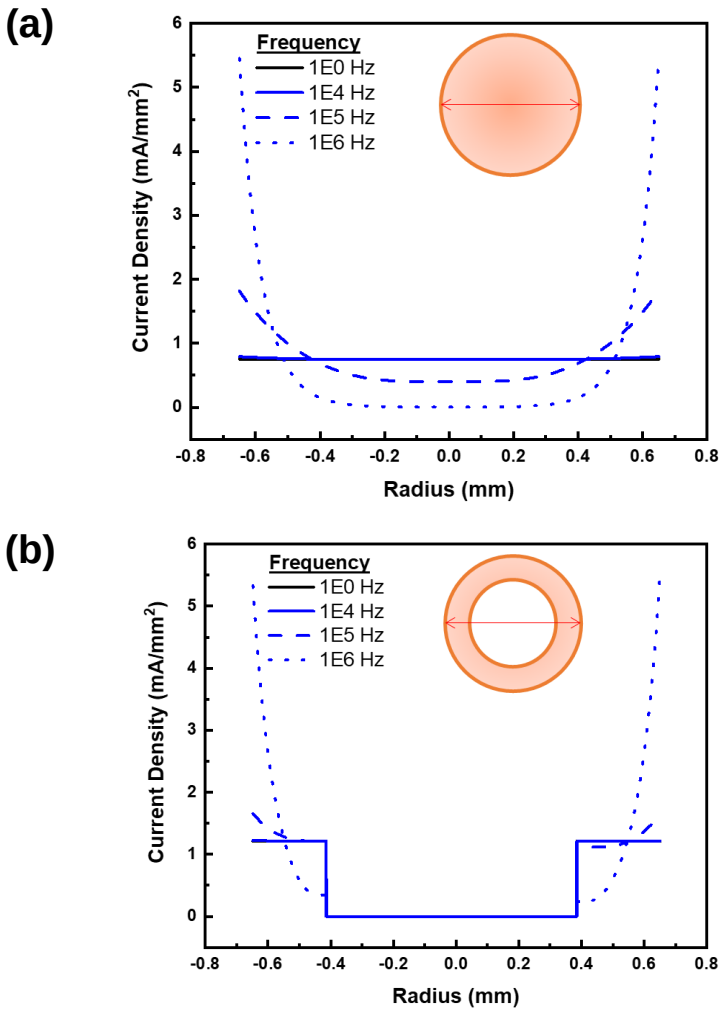


**Figure 1.3:** **Current density across the diameter of conductor for a solid conductor (top) and a hollow conductor (bottom). Frequencies of 1E0 Hz and 1E4 Hz are overlapping in the graph. Values between 1E2 and 1E3 were omitted as they would have overlapped as well.**

## 1.4. Generating Core-Shell Structures and Coaxial 3D Printing

A core-shell structure, or a hollow conductor, is effectively a tube. The printing of such structures has been described as core-shell printing or coaxial printing in the literature.[18] Coaxial printing has been demonstrated primarily in biomedical applications and in bioprinting, where the core-shell structure mimics the tubular structures found in biological systems.[19], [20] The use of core-shell materials has also been demonstrated in 3D printed parts. Generally, the core provides strength and rigidity to the filament whereas the shell provides interlaminar adhesion. Such examples of core-shell systems can be

found in the printing of carbon fibre reinforced filaments[21] and as composites to increase the printability of more challenging plastics.[22] A coaxial nozzle is often the most used method of generating core-shell structures. However, it is possible to prepare the core-shell filament before printing. In addition, the use of polymerization-induced phase separation shows a unique case of generating conductive core-shell structures.

### 1.4.1. Coaxial Nozzle

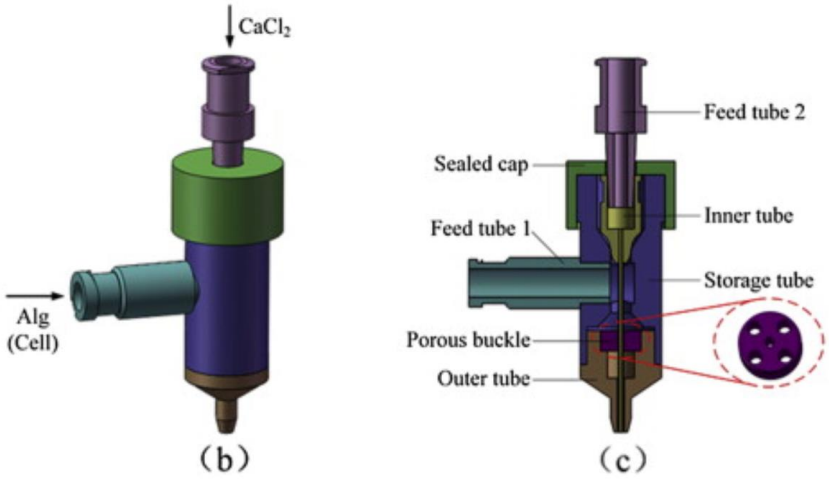


**Figure 1.4: Coaxial nozzle for printing hollow alginate tubes. Reprinted with permission [19], Copyright © 2015 Elsevier Ltd. All rights reserved.**

The most versatile and common approach to coaxial printing would be through a specially designed coaxial nozzle. Such a nozzle takes two material inputs (figure 1.4, feed tubes) to generate the structure. These nozzles generate a core-shell “filament” during the printing process, *in situ*. Because two different materials are fed directly into the nozzle, these nozzles allow for flexibility in the phase of the input materials: liquid-liquid, solid-solid, liquid-solid, or solid-liquid. Caution does need to be taken in dispensing the two materials to ensure that the shell surrounds the core material, and the core material forms a complete jet (figure 1.5). If the surface tension of the core fluid is too high, a series of discontinuous droplets arises (figure 1.5b) described as the Plateau-Rayleigh instability. If drag force is sufficient to prevent the formation of droplets, a continuous jet emerges

(figure 1.5c). Overall, in some cases, consideration of the interfacial phenomena of the input materials is required.

In contrast, the use of a prefabricated core-shell filament limits the inputs to primarily solid-solid but does result in greater simplicity during printing.

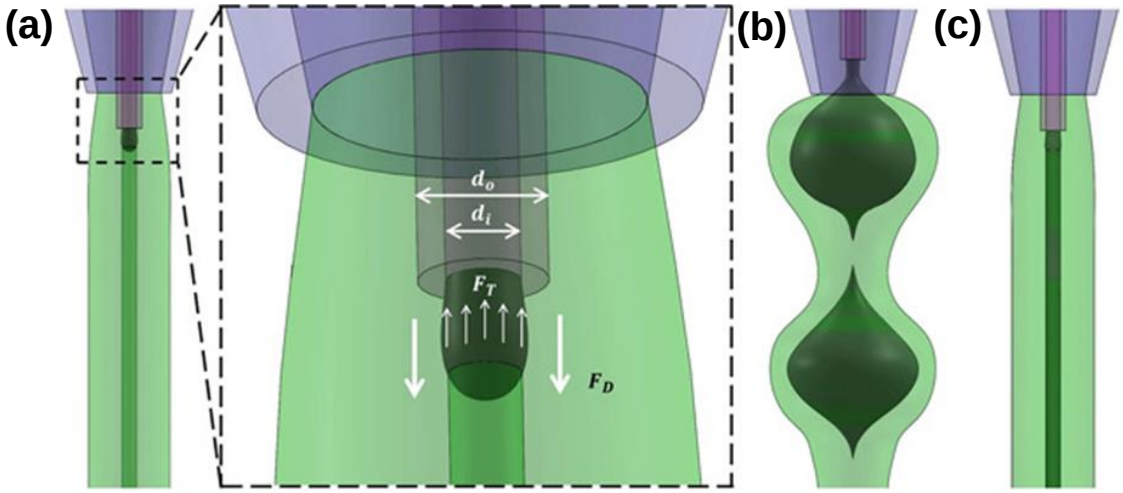


**Figure 1.5: The coaxial printing process requires balancing the surface tension (FT) and the drag force (Fd) (a + insert). If the surface tension is too high, droplets form (b). If viscous drag is correct, a smooth jet occurs (c). Reprinted with permission[23], Copyright © 2019 WILEY-VCH Verlag GmbH & Co. KGaA, Weinheim**

## 1.4.2. Core-Shell Filament

An alternative approach would be to generate the core-shell filament before printing (figure 1.6). Here the pre-prepared filament can be stored for later and printed using a conventional nozzle system/printer without modification. Thus, the technique is widely applicable and simplify the printing process of coaxial filaments. However, because the filament is to be stored, both materials, core, and shell inputs, need to be solid at room temperature to ensure stability. Thus, such an approach would not be amenable to the use of conductive pastes.

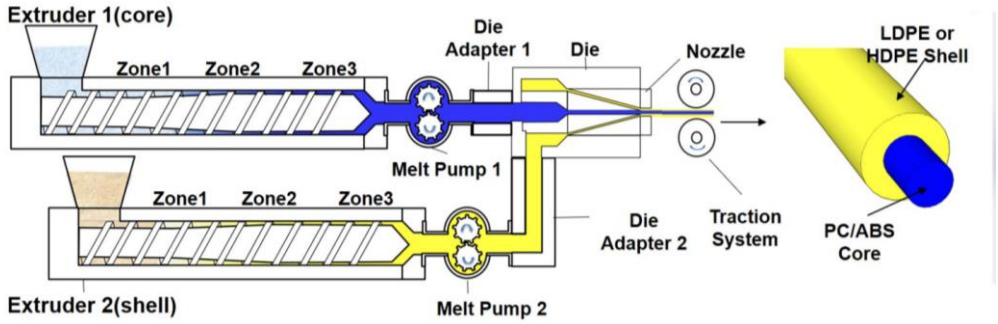


**Figure 1.6: Preparation of core-shell filament for 3D printing. Reprinted with permission from [22], Copyright © 2019, American Chemical Society.**

There does exist a few examples of a conductive shell paired with a non-conductive core. There is one example found in the literature where the use of polymerization-induced phase separation (PIPS) was used to generate conductive silver 3D structures.[24] By tuning the gelation rate and crosslinking density of the photocurable resin, it is possible to tune the distribution of silver in the final print from “composite” to a “silver coating” (figure 1.7). At low crosslinking density and slow gelation, the dissolved silver in the resin can diffuse to the surface where it is later cured. Diffusion is slowed at higher crosslinking and gelation rates resulting in either a gradient from the surface or interspersed silver in the final print.

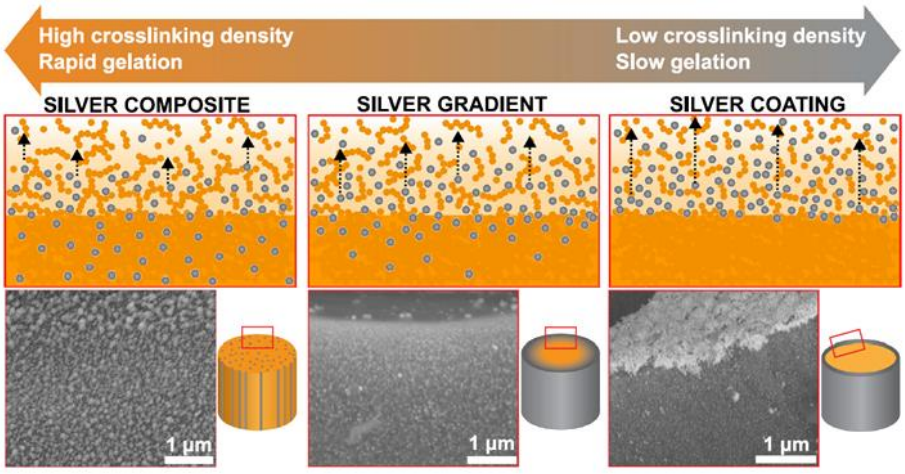


**Figure 1.7: Careful control of the diffusion of silver in photocurable resin affects the distribution of silver in the final product.[24] Open access Copyright © 2021, Crown**

Overall, the PIPS method of conductive core-shell printing is promising, but it is not quite able to be used in the efficient 3D printing of electronics. Because this method relies on SLA and a photocurable resin, it would be difficult to print structural and embedded electronic systems.

## 1.5. Structural & Embedded Electronics Systems, 3D Printing Electronics & Wireless Power Transfer

With the development of advanced multi-material 3D printing, it has become possible to print fully integrated and embedded electronic systems.[25]–[27] Multi-material 3D printing has allowed for the printing of the substrate, or structure, of an electronic system and the conductive traces. Some systems also incorporate a pick-in-place system to add electronic components such as transistors and integrated circuits, further increasing what is accessible with the technology. To date, the 3D printing of electronics has been shown in the manufacturing of structural electronics,[28], [29] fully interactive electronic systems[30] and printed circuit boards.[31]

The advantage of multi-material 3D printing is in its ability to reduce material consumption either due to efficient preparation of conductive traces, such as with circuit boards, or in reducing the overall material consumption as in the case with structural and embedded electronic systems. In the production of circuit boards, much of the initially deposited copper is etched away during processing.[13] With a 3D printing approach, conductive material is only deposited where it is needed thus minimizing wasted generation. Figure 1.8 summarizes conventional PCB manufacturing and 3D printed circuit board manufacturing.

Circuit boards prepared by the conventional process undergo a series of wet chemical processes, the etching step alone annually generates $1x10^{12}$ litres of spent solution and recovering waste copper from etchant is of ongoing research.[32]–[35] Ideally, minimizing that waste is the preferred solution. With 3D printing-based approaches, the necessity of lithographic etching is eliminated as conductive material is deposited only where it is required.

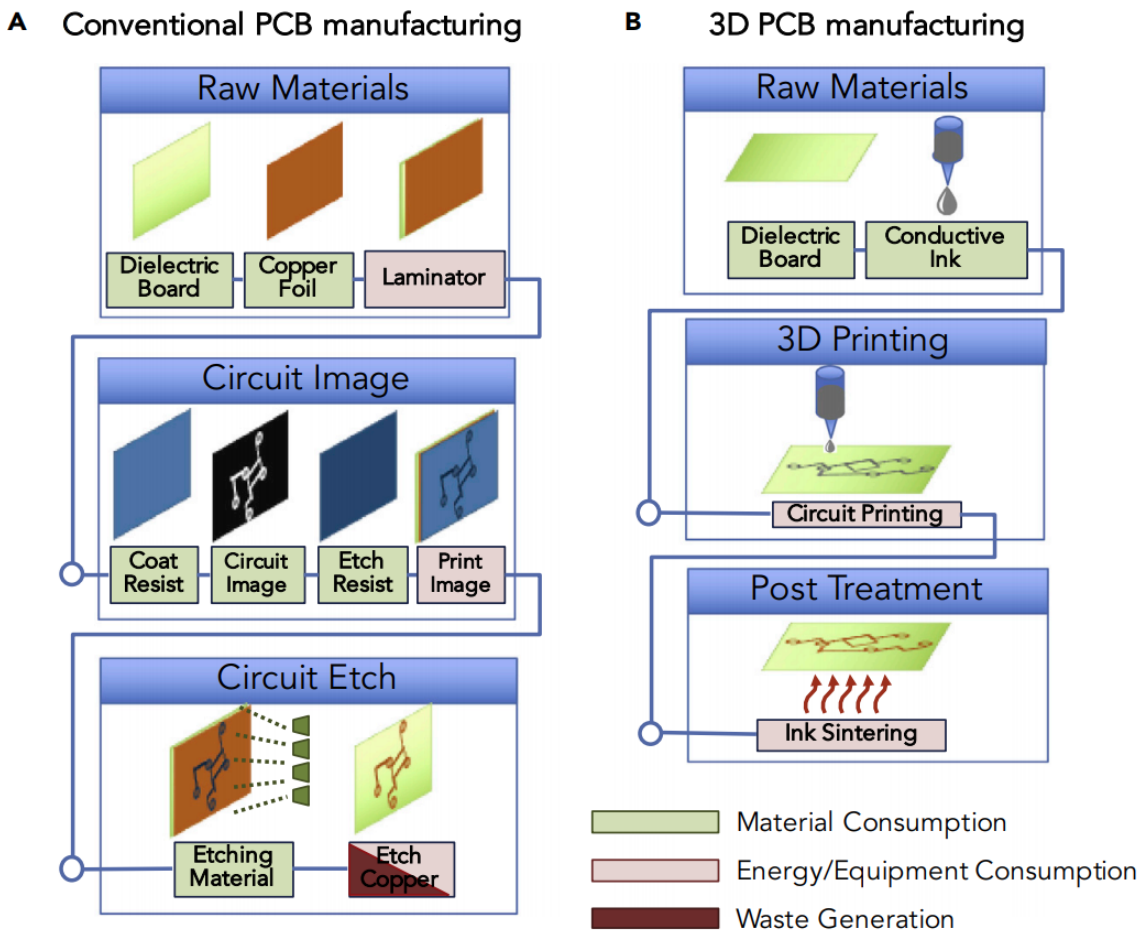


**Figure 1.8: Comparison of conventional PCB manufacturing (A) and a 3D Printing approach to PCB manufacturing (B). Reprinted with permission[13], Copyright © 2018 Elsevier Inc.**

Additionally, 3D printing reduces material consumption in the production of structural and embedded electronic systems. In these structures, electrical components are embedded within the structure itself, minimizing space. The use of embedded passive components, such as resistors, capacitors, and inductors, allows for multi-layer circuits, thus reducing the footprint of a circuit. Some examples include fully customized lights, microwave electronics, fully interactive and lightweight devices.[30] In these cases, much less material is required because the substrate is the fabricated object. Figure 1.9 shows a digital egg-shaped timer with embedded interconnections and components. The structure was prepared through fused filament fabrication, conductive pasted was used for the interconnects, and pick and place technology was used to position components.

In general, 3D printing of structural electronics[36] commonly uses a combination of fused filament fabrication (FFF) for the substrate, and direct-ink-writing (DIW) for the conductive traces.

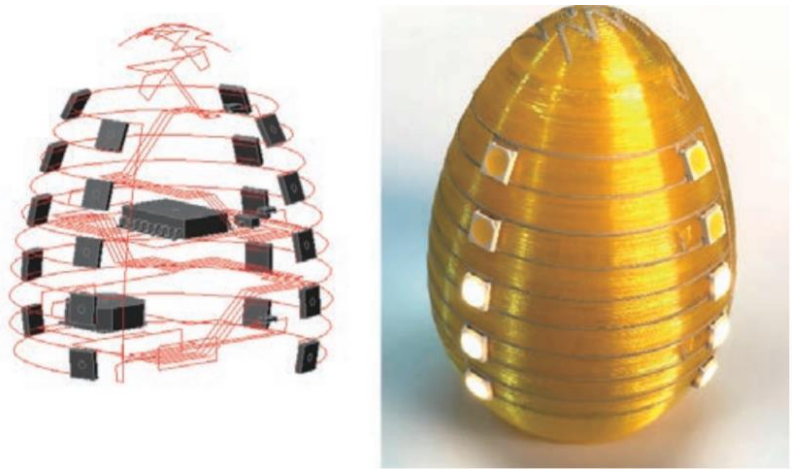

**Figure 1.9: Selected examples of structural electronics. An electric egg timer (a) is shown with embedded components. Reprinted with permission [37], Copyright © 2019, IEEE.**

### 1.5.1. Structural Electronics – Substrate

The main substrate for circuits in structural electronics is plastic. In general, these plastics can be either a thermoset or a thermoplastic which will determine the printing process used to generate the structure. Most commonly, a photo-based 3D printing technique, such as stereolithography (SLA), or a heat-based deposition method, such as fused deposition modelling (FDM) and fused filament fabrication (FFF), are used.

Photo-based 3D printing techniques use light to initiate crosslinking in a photocurable resin to generate the layers of a 3D structure. These methods have the advantage of offering greater resolution in structural electronics[38] compared with thermal-based polymer extrusion. However, photo-based 3D printing is not without its shortcomings. The photocurable acrylate resins used in SLA, and related photo-based 3D printing techniques, undergo changes in mechanical properties under elevated temperatures and short-wavelength, ultraviolet, irradiation.[39] In addition, owing to their nature as thermosets, cured plastics cannot be easily repaired, thus a photo-based approach may not be ideal for creating long-lasting and durable structural electronics.

Conversely, FDM and FFF deposit layers of thermoplastic to form a 3D structure. In most cases, FDM and FFF are interchangeable as the difference between the two is small. In 1989, Stratasys filed the patent for fused deposition modelling (FDM),[40] however, in 2009 the patent expired(Patent #: US005121329). Since then, fused filament fabrication (FFF), which is the untrademarked name for a similar process of thermal-based polymer extrusion, has become widely available. In general, this technique uses thermoplastics, such as poly-lactic acid (PLA), because these plastics can be melted and solidified without compromising the mechanical properties of the plastic. The benefit of using thermoplastic is that it can be repaired due to the physical properties of the plastic. In cases where a higher resolution of printing is required for an application, an increased resolution has been shown through the additional use of high-resolution subtractive techniques[25] used in tandem with FFF. In addition, wires can be embedded into thermoplastic and can be used in combination with other techniques.[25] Though the thermoplastics are not as robust as many of the resins available and substrates used for printed circuit boards, they are one of the few materials cheaply and easily printed.

### 1.5.2. Structural Electronics – Conductive Traces

To connect components within a 3D printed electronic structure, conductive traces are required. Wire, in some cases, can be embedded into the system itself,[25] or a conductive material can be printed along during the printing of the substrate. There are two common approaches to introducing conductive material: fused filament fabrication (FFF) and direct-ink writing (DIW).

In fused filament fabrication, a conductive filament is used to print the required traces. Conductive filaments are generally a thermoplastic composite with either metal powder or carbon, in the form of graphene or fibre.[30], [41]–[43] However, these filaments are orders of magnitude less conductive than pure metal. This limitation arises because of poor loading of conductive filler into the thermoplastic matrix. More conductive material results in poor to no printing performance which arises because printability decreases with increased filler loading. The most conductive thermoplastic filament that could be found, which used copper-silver nanowire as the conductive filler, only achieved conductivity of $5 \times 10^2$ S/cm.[44] Alternatively, low-melting alloys are printable and have been demonstrated, but such materials are challenging to work with and may not suit every application.[45] Regarding electronics and electronic manufacturing, these high

resistances are undesirable and result in high Ohmic losses. Therefore, a more conductive material is preferred, such as a conductive ink or paste.

Direct-ink writing uses an ink the material feedstock. Despite the term ink, the material used often leans toward being more like a paste and is often a viscoelastic fluid. Viscoelastic fluids exhibit both viscous and elastic strain in response to deformation. For proper printing, the paste also needs to exhibit shear thinning, analogous to the melting of a plastic. Shear-thinning, or thixotropic, pastes exhibit a solid-like property when under zero shear, however, upon experiencing a shear force, the force within a nozzle, the paste behaves more like a fluid: they flow because of a decrease in viscosity. The paste remains in place once extruded because removal of the shear force results in the return to a more solid-like behaviour.

Conductive DIW pastes are comprised of a precious metal, silver nanoparticles and or silver micro-flakes. Less precious metals, such as copper can be used. However, because of their higher reactivity, these metals tend to oxidize under ambient conditions, even after curing. Oxidation reduces conductivity over time and can result in a non-conductive trace if enough oxidation has occurred. In addition, copper pastes during processing require either high heat and or reducing atmospheres, such as hydrogen gas or formic acid vapour, for proper sintering.[46] These atmospheres are hazardous, require appropriate safety measures and equipment for their use, and generally offset much of the cost savings of using copper. Additionally, many copper inks require toxic formate salts or require copper nanoparticles, which are themselves synthesized from formate salts, for proper sintering.[47]–[49] Silver pastes can benefit from the incorporation of silver nanoparticles, however, their inclusion is not strictly required. Thus, silver is generally preferred in conductive pastes as it is facile to work while offering reasonable conductivity: silver paste has a conductivity above $10^4$ S/cm.[26] Silver pastes can also be cured under generally mild conditions.

However, silver, being a precious metal, can be prohibitively expensive, and thus it is desirable to reduce its consumption for the more sustainable production of structural electronics. Depending on the application, it is possible to reduce the amount of silver used in a conductive trace without negatively impacting the conductor. Because of the skin effect, the core of a conductor can be carrying no current and thus can be replaced. This kind of conductor would be most useful in high frequency applications such as

inductive coupling and wireless power transfer. However, it is worth noting, that a sheath conductor could still be used in place of a conventional solid conductor.

### 1.5.3. Inductors & Wireless Power Transfer

Inductors are an important component in power and communication.[50] The 3D printing of inductors has been demonstrated through the use of conductive filament,[51] silver paste,[52] low-melting alloys,[53] and electroless plating.[54] Core-shell printed inductors would function well in wireless power transfer applications as the efficiency increases at higher frequencies.

Inductors themselves are passive components that store energy in their magnetic field, in contrast to capacitors which store energy in their electric field. Fundamentally, all wires have inductance and can be regarded as inductors. However, to be of practical use, wires are shaped in such a way to maximize their inductance. The total inductance of a wire can be thought of as the sum of the self-inductance and all mutual inductances.[55] Mutual inductances can be positive or negative, depending on the interaction. Segments of adjacent parallel current-carrying wire have a positive mutual inductance whereas segments with an anti-parallel current flow have negative inductance.

Inductors can take the shape of a coil of wire-shaped around a core. The core can be air, but in some cases, a ferromagnetic core is preferred as it increases the inductance of the inductor. In circuits, planar designs such as a rectangular spiral or circular spiral are preferred, however, this depends on the target application. Rectangular spirals do have a higher inductance than circular spirals,[55] but for power transfer application, circular spirals tend to have better coupling.[56]

For a circular spiral, the main parameters determining the inductance are the width (w), the spacing (s), the inner diameter ($D_{in}$) and the total diameter or outer diameter of the spiral ($D_{out}$) (figure 1.10), in addition to the number of revolutions. The thickness, or height, of a planar inductor, has minimal impact on the final value and is usually not regarded. These parameters can be modified to adjust the final inductance of the inductor and will modulate how well power transfer occurs wirelessly.

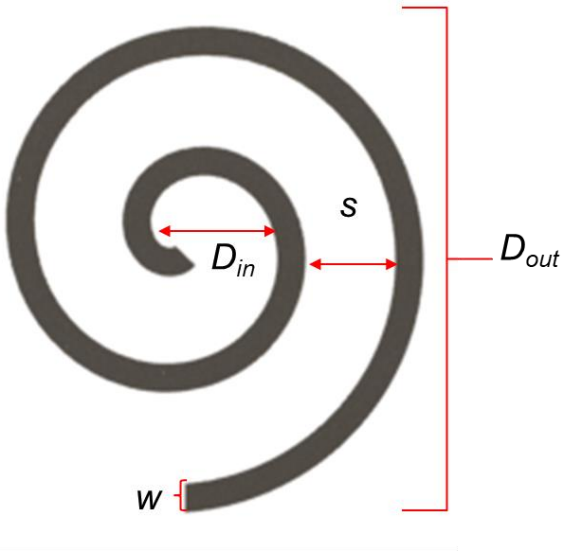


**Figure 1.10: Overview of planar spiral inductor and major parameters.**

Wireless power transfer (WPT) can be thought of as the ability to transmit electrical power from one place to another without the use of a wire or other conductive media. The use of WPT can be advantageous in the case of powering biomedical implants where replacing the battery may be undesirable, e.g., a pacemaker.[57] Categorically, WPT can be divided into “near-field” and “far-field” transfers, which depend on the distance of transfer (figure 1.11). The separation between near and far is vaguely defined.[58] Generally, near field WPT is on the order of centimetres whereas far-field can included distances in the range of kilometres.[59] In the near-field WPT range, inductive coupling has grown to become one of the most prolific methods finding applications in areas such as electronic systems, implants, and security systems.[60]

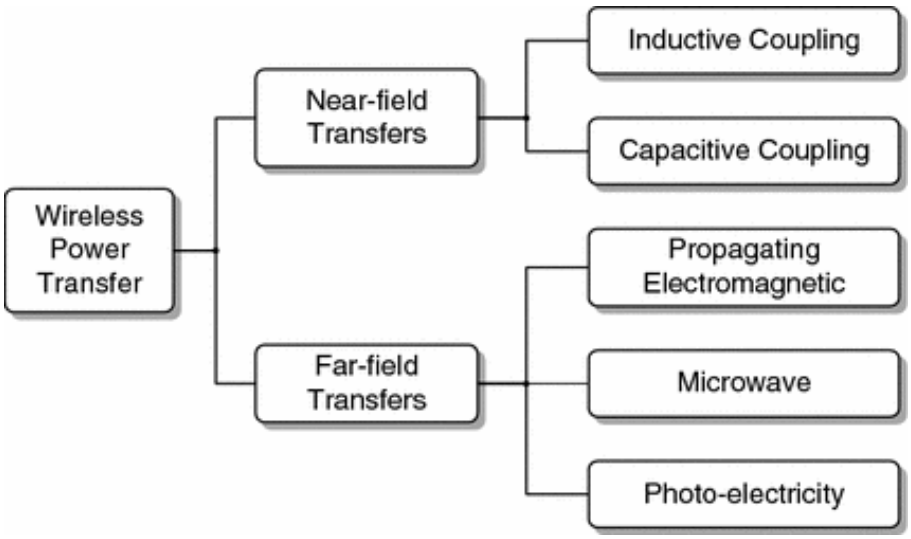


**Figure 1.11: Categories of wireless power transfer. Reprinted with permission [61], Copyright © 2013, Springer Science Business Media New York**

An inductive coupling system consists of two coils, a transmitting coil, and a receiving coil. A power amplifier supplies the transmitting coil with an alternating current which generates a time-varying magnetic field as described by Ampere's law. This time-varying magnetic field induces an alternating EMF in the receiving coil as described by Faraday's law of induction. Together, the two coils act like a transformer. The effectiveness and efficiency of this power transferred are captured in the coupling coefficient, k, and the maximum power transfer efficiency, $\eta_{max}$.

The more magnetic flux through the receiving coil in an inductive power transfer system, the more power that can be transferred.[61] The coupling coefficient, or coupling factor, is a dimensionless measure of how well two coils are coupled. The coupling coefficient ranges from 1 (perfect coupling) to 0 (no coupling), though some extend the range to include -1 indicating perfect negative coupling.

The coupling coefficient is a measure of how well two coils are coupled and is calculated by equation 1.5 where M is the mutual inductance and $L_1$ and $L_2$ are the inductances of the two coils in isolation. An alternative way of determining the coupling coefficient is shown in equation 1.6. This measurement is conducted with the two coils in close contact. $L_s$ is the measured inductance across $L_1$ with $L_2$ shorted. $L_o$ is the inductance of $L_1$ with $L_2$ left open.

$$k = \frac{M}{\sqrt{L_1 L_2}} \tag{1.5}$$

$$k = \sqrt{\left(1 - \frac{L_s}{L_o}\right)} \tag{1.6}$$

The main factors that affect the coupling coefficient are the ones that influence mutual inductance. Therefore, the proximity of the two inductors (z) and the size difference between the coils (figure 1.12) are contributing factors. Perfectly aligned coils with minimal separation and as equal size as possible will result in a higher coupling coefficient.[61] In addition, the addition of a magnetic backplane can help increase the coupling coefficient.[62], [63] Figure 1.13 illustrates how the introduction of a magnetic backplane helps focus the magnetic field lines from the transmitting coil. Thus the magnetic field lines become more confined, thus increasing the coupling coefficient and the power transfer efficiency.[64] Overall, optimizing the coupling coefficient is important in achieving high-efficiency WPT inductive coupling systems.

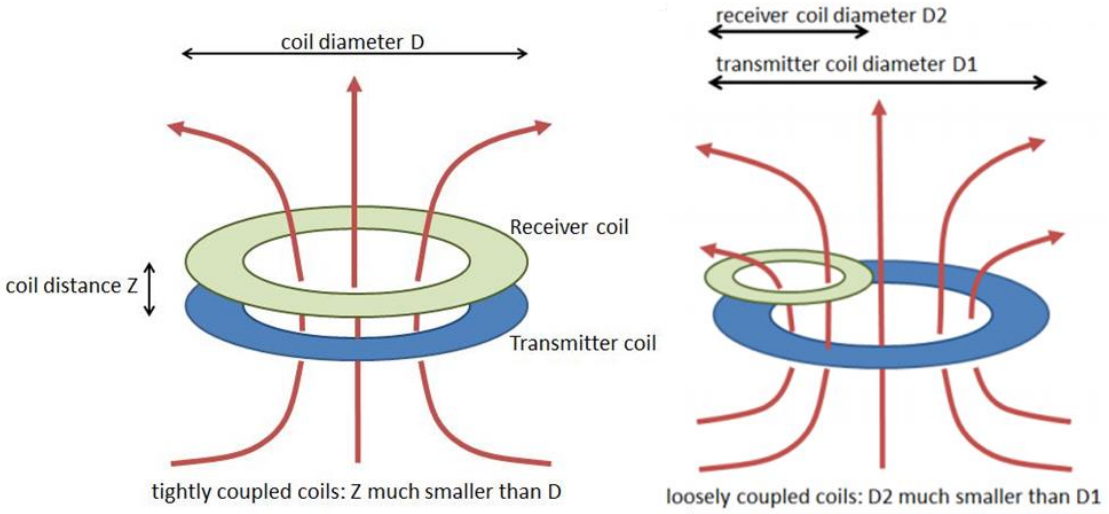


**Figure 1.12: Factors influencing coupling factor. Reproduced with permission**[65] **Copyright © 2021 Wireless Power Consortium, Inc.**

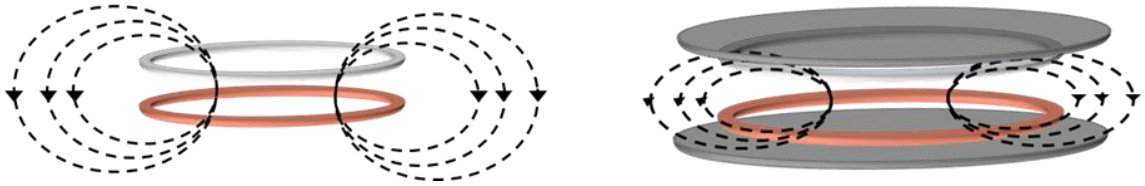

**Figure 1.13: Magnetic field lines between two coupled coils without a backplane (left) and with a backplane (right).**

In wireless power transfer systems, the coupling coefficient is not the transfer efficiency, but it is related to the efficiency. The maximum power transfer efficiency ($\eta_{max}$) of two inductive coupled coils can be calculated using equation 1.7 where k is the coupling factor of the two coils and Q is the quality factor of the transmitting coil (1) and receiving coil (2).[66] In addition to the coupling coefficient, the quality factor of the individual inductors plays an important role. The quality factor, Q, is related to the frequency of operation (f), the inductance of the inductor (L), and the DC resistance (R). A high Q means that little energy is lost relative to the stored energy (equation 1.8).

$$\eta_{max} = \frac{k^2 Q_1 Q_2}{(kQ_1 + k^2 + 1)(kQ_2 + 1)} \tag{1.7}$$

$$Q = \frac{2\pi f L}{R} \tag{1.8}$$

# Chapter 2.

# Design of Core-shell Nozzles

As discussed in section 1.4, there are two primary methods for conducting core-shell printing: the use of a coaxial nozzle (1.4.1) or filament (1.4.2). Conductive core-shell printing also has been demonstrated. The core material consists of a conductive low-melting metal alloy and was used for the printing of electronic components and sensors; [23], [53] however, using a conductive shell and an insulating core has not been reported yet. Because for this thesis, a conductive shell was needed, a coaxial approach was chosen.

## 2.1. Objective and Plan for Core-Shell Nozzle Design

For core-shell printing, it was decided that a non-conductive thermoplastic would be used as the core material to provide support. Air, in theory, could be used but would be more difficult to realize. Material extruded during the 3D printing is a viscous fluid that would collapse under its weight upon extrusion: the conductor would not remain hollow after printing if air were used. Because a support material would be required for the paste, thermoplastic seemed an ideal core material.

The design for the nozzle was such that thermoplastic and conductive paste could be printed coaxially to generate the sheath conductor. This main body of the nozzle consisted of a hot end like commercial ones for FFF, but it was enlarged to accommodate space for the paste and the shell. An inner needle was used to guide the molten thermoplastic to the end of the nozzle with the nozzle being designed around the inner needle to shape the paste to form the shell. The design was constrained by the limits of manufacturing, but consideration was made to the skin depth of the printed conductor.

### 2.1.1. Skin Depth

As mentioned previously, current density is more concentrated at the surface of a conductor at higher frequencies. In designing our nozzle, the skin depth at 2 MHz, the maximum that could be measured in the lab, for a silver paste was calculated and guided the design. Based on equation 1.2, at a frequency of 2 MHz, the skin depth for a printed

conductor (silver paste conductivity ~ $10^4$ S/cm[26]) would be approximately 250 µm. As current density rapidly drops off after 1 skin depth, effectively any material beyond 250 µm can be replaced with non-conductive or less conductive materials, without a dramatic change to the current density distribution.

### 2.1.2. Machining and High-resolution 3D Printing

Some structures are not easily manufactured, especially with the dimensions desired for the coaxial nozzle. There were several discussions with Mustafa Sajid from the School of Mechatronics System Engineering at SFU about what would be possible to machine and what would be a challenge. These discussions influenced how the coaxial nozzle was designed. One key element that would not be possible to machine was the inner needle of the coaxial nozzle. This needle would be essential to reduce the input filament (1.75 mm) to a final, much narrower diameter. Instead, a commercial needle was fitted inside the nozzle to reduce the size of the thermoplastic filament from 1.75 mm to 0.5 mm. The remaining portion of the nozzle was designed to accommodate paste flow and house the needle. The use of 3D printing allowed a similar nozzle design to be printed as a single unit, without the need for an external needle.

## 2.2. Nozzle Prototypes

Three prototypes were considered during the process, but only one was used for subsequent experiments. In brief, prototype 1 and prototype 2 were made with an aluminum body and a modified stainless-steel needle. Carima, South Korea, supported the 3D printing of prototype 3, an all-plastic construction.

For the aluminum nozzles, milling was used to prepare the overall shape. Finer detail such as the threads and holes for the paste and filament were machined using a lathe. Overall, this produced high-quality nozzles for 3D Printing. However, in the process of designing the nozzles, the use of 3D printing to prepare the nozzles was considered.

A photo-based 3D printing technique was also used to produce a plastic prototype. Photocurable resin-based 3D printing, for example, SLA, has a high resolution on the order of tens of microns. The added benefit of using 3D printing is that it allows for rapid prototyping of multiple nozzles for additional tests. With the use of multiple nozzles, it

would be possible to further refine the nozzle design for optimal printing. However, as will be discussed later, these nozzles were not successful.

### 2.2.1. Thermal Simulation

Thermal simulations were conducted on the prototypes because it was found that prototype 1 did not behave as expected. These thermal simulations were conducted using the COMSOL Multiphysics (5.5) Heat Transfer in Solids module with a stationary or time-dependent solver. The heat flux boundary was set to approximate the resistors in the nozzle. For the aluminum nozzles, prototypes 1 and 2, a heat flux of 40W was used to approximate experimental conditions. For the plastic nozzles, a total heat flux of 10 W was used to match experimental conditions; using a total power of 40W to heat the plastic nozzle resulted in the nozzle cracking under the thermal load. The simulations were conducted in air at room temperature (293.15 K). Default material parameters were used unless otherwise stated.

The thermal simulation conducted, “Heat Transfer in Solids”, considers equations 2.1-2.3. Equation 2.1 represents the stationary case where ρ is the density of the solid, $C_p$ its heat capacity at constant pressure, **q** the heat flux vector, **u** the velocity field (if parts of the model are moving), Q is the heat source, k the solid thermal conductivity and T the temperature. In a time-dependent simulation, equation 2.3 must be considered instead of 2.1. In a stationary system, the first part of equation 2.1 is zero. Equation 2.3 considers the thermoelastic dampening, $Q_{ted}$.

$$\rho C_p \boldsymbol{u} \cdot \nabla \mathrm{T} + \nabla \cdot \mathbf{q} = Q + Q_{ted} \tag{2.1}$$

$$\boldsymbol{q} = -k \nabla T \tag{2.2}$$

$$\rho C_p \frac{\partial T}{\partial t} + \rho C_p \boldsymbol{u} \cdot \nabla \mathrm{T} + \nabla \cdot \mathbf{q} = Q + Q_{ted} \tag{2.3}$$

### 2.2.2. Nozzle Prototype 1

Prototype 1 (figure 2.1) was the first nozzle designed. It was comprised of a threaded aluminum body with a small side opening designed for paste. The overall design is larger than a traditional FFF 3D printing nozzle. The larger size was to accommodate the needle as well as the paste. In addition, it was thought that the larger size would increase the separation between the paste and the hot resistors. Because the paste does contain volatile organic solvents, it would be better to increase the separation. However, the large size may have become a problem during the printing process as when this nozzle was first manufactured and tested for printing, it was found that the printing of thermoplastic did not proceed smoothly. The nozzle was quick to cool and did not hold heat well enough to sustain the flow of thermoplastic filament. A thermal simulation was done to investigate the heat distribution of the nozzle.

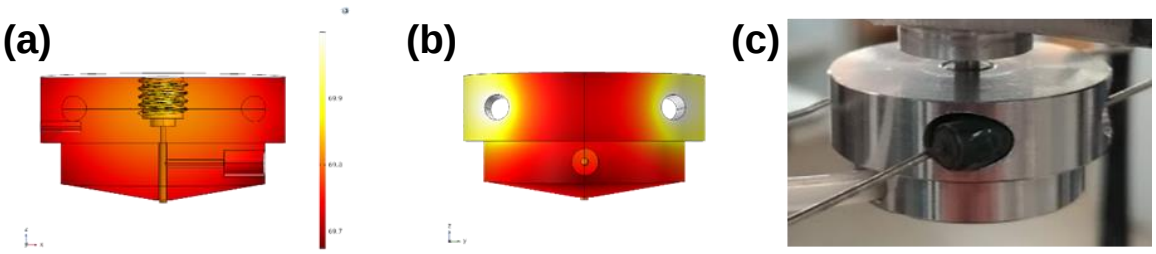


**Figure 2.1: Thermal simulation (a,b) and actual nozzle of prototype 1 (c). The internal portion of the nozzle is shown in (a) and the front in (b).**

It was found that the thermal profile of this nozzle was not very uniform. Most of the heat in this nozzle was concentrated primarily around the two resistors (the openings near the top). As well, the inner needle did not receive much heat. Consequently, the molten filament would cool down and become viscous as it was passing through the needle resulting in a poor thermoplastic flow. Overall, this poor heat distribution resulted in poor print quality of the nozzle.

It was thought that the large size of the nozzle resulted in rapid cooling and poor heat distribution. A larger design was initially considered to increase the distance between the heating resistors and the paste channel; thus, a smaller design was considered for a second prototype.

### 2.2.3. Nozzle Prototype 2

Prototype 2 (Figure 2.2) was designed and manufactured in the same way as prototype 1, however, the design was made more compact. This design change resulted in a more uniform heat distribution across the nozzle as seen from the simulation data (Figure 2.2a). Additionally, the inner needle of prototype 2 is kept hotter than the needle in prototype 1. This better distribution of heat resulted in a better extrusion rate and print quality. The nozzle did overall have a better flowrate of thermoplastic which resulted in significantly better print quality. Thus, this nozzle was used in subsequent experiments.

However, it was found that the sheath conductor (core-shell filament) generated by this nozzle was not perfectly centred (Figure 2.3). Thus, high-resolution 3D printing techniques were considered at increasing the concentricity of the nozzle and the overall print quality.

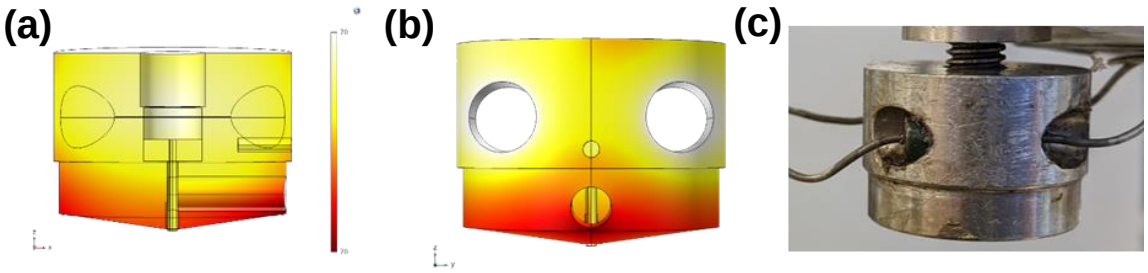


**Figure 2.2: Thermal simulation (a,b) and actual nozzle of prototype 2 (c). The internal portion of the nozzle is shown in (a) and the front in (b).**

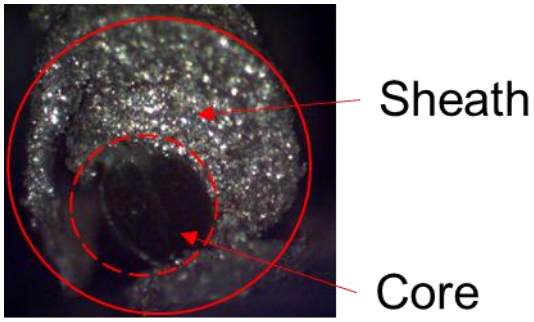


**Figure 2.3: Core-shell filament (sheath conductor) generated by prototype 2.**

### 2.2.4. Nozzle Prototype 3

Prototype 3 (Figure 2.4) was a slightly modified version of prototype 2 and printed in plastic. It is known that plastic resins for 3D printing have poor thermal conductivities and

decompose when heated. However, thermal simulations did suggest that the plastic nozzle, at thermal equilibrium, would become hot enough to extrude filament without decomposing, thus it was pursued.

The use of a 3D printed nozzle would also have been a novel demonstration, and additionally useful overall. Because of the rapid nature of 3D printing and low cost, multiple variations of the nozzle could be made to optimize the core-shell printing process. Additionally, the ability to print custom nozzles would open new and different research opportunities. Thus, in addition to the two aluminum nozzles, six varying designs of plastic nozzles were prepared.

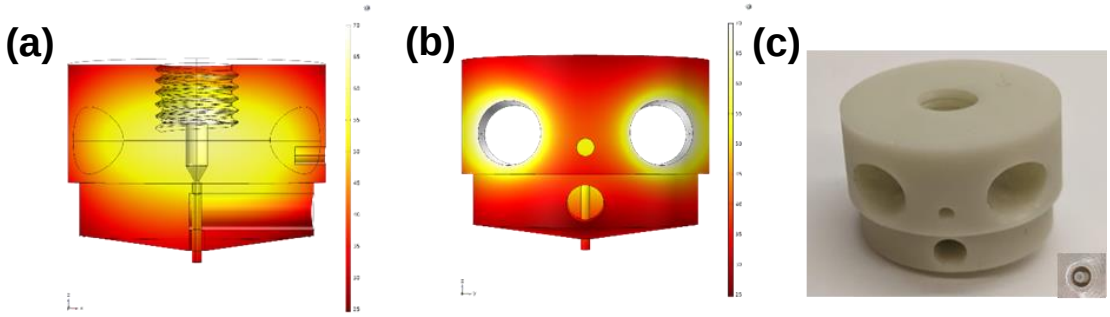


**Figure 2.4: Thermal simulation (a,b) and actual nozzle of prototype 3 (c). The internal portion of the nozzle is shown in (a) and the front in (b).**

However, the nozzles could not print the filament. Despite being hot enough to melt polycaprolactone filament, the nozzle was unable to extrude the filament. During extrusion, the nozzle would fracture in half due to presumably loads on the material. It was thought that the plastic material used was too brittle for proper printing.

In the future, it would be worth pursuing such 3D printed nozzles, as custom nozzles could be printed reasonably quickly and cheaply. However, careful material selection and design would be required to ensure that the nozzles are sufficiently robust for 3D printing. In addition, these plastics would need to be thermally stable to allow for the printing of high-strength thermoplastics and have sufficiently high thermal conductivity to allow for fast 3D printing. Unfortunately, such material does not yet exist, and further research will be required to allow for the 3D printing of FFF nozzles.

# Chapter 3.

# 3D Printing with Core-Shell Nozzles

## 3.1. Sustainability in Sheath Conductors

The use of a sheath conductor is expected to decrease the amount of conductive material in the final printed inductor. The theoretical material savings afforded by a single, double, and triple width core-shell inductor have been tabulated in Table 1 of which designs are detailed section 3.2. These values were calculated from the CAD files based on the expected dimensions of the final inductors. These values represent an ideal case of material “savings;” any material that is not shell is much cheaper thermoplastic. For perspective, the silver flake used costs 2.5 CAD $/g whereas the filament costs about 0.03 $/g. Based on the tabulated results, the ratio between core and shell is 45%, or one-third of the silver paste has been saved in this inductor.

These hypothetical results are also based on a nozzle with an outer diameter of 1.3 mm and a core of 0.5 mm which results in a shell thickness of 400 µm. Based on the skin depth calculations in section 2.1.1, the shell can be made even thinner without significantly impacting the electrical properties of the conductor. In addition, the entire nozzle diameter could be further reduced to reduce the amount of material being extruded. The generated coaxial nozzle was constrained by machining requirements, however, with high-resolution 3D metal printing, it could be possible to design and fabricate a nozzle with a thinner shell.

Exaddon has developed the CERES printing system which is capable of printing pure metal at the micrometre scale.[67] The company boasts an XY resolution of 250 nm and a Z resolution of 5 nm which would allow for high precision fabrication. Such nozzles could have the potential to further reduce the amount of silver paste consumed by both narrowing the nozzle diameter and the shell thickness.

**Table 1: Theoretical calculation of material savings for the core-shell printed inductors based on estimated values and designs.**

| Width | Total Volume ($mm^3$) | Core Volume ($mm^3$) | Shell Volume ($mm^3$) | Core to Shell Ratio |
|---|---|---|---|---|
| Single | 15.28 | 4.24 | 11.03 | 37% |
| Double | 40.80 | 12.36 | 28.43 | 43% |
| Triple | 78.07 | 24.40 | 53.67 | 45% |

## 3.2. Printing Process

Printing was carried out the Orion DeltaTM desktop 3D printer from SeeMeCNC®, outfitted with the coaxial nozzle. Paste was either manually fed into the nozzle or supplied by the DISCOV3RY paste extruder produced by Structur3D. Because of material selection, the print temperature was set at 80°C. Print speed was maintained at 0.6 mm/s with a layer height of 0.2mm. Figure 3.1 shows the printer setup.

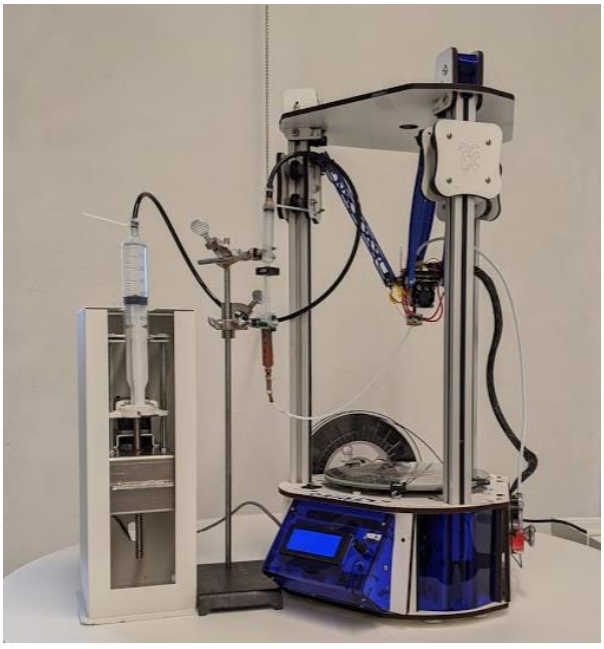

**Figure 3.1: Core-shell 3D printer setup.**

### 3.2.1. Inductor Design

As described in section 1.7.1, the main parameters determining the inductance of planar spiral inductors are the width (w), the spacing (s), the inner diameter ($D_{in}$) and the total diameter or outer diameter of the spiral ($D_{out}$). For this work, three similar inductor designs were considered. For these three the inner diameter and the spacing were maintained at 1.3 mm and 1.5 mm, respectively. The three designs differ in their width of the conductive trace and their outer spiral diameter. The three designs are shown in figure 3.2 and have been exaggerated to illustrate their core-shell nature.


**Figure 3.2: CAD renderings of the three designs. Thickness has been exaggerated to emphasize the core. Single, double and triple widths (a,b,c respectively) are shown.**

### 3.2.2. Shell Material Selection and Preparation

For the conductive shell, either a conductive filament could be used or a conductive paste. Conductive filaments overall have a lower conductivity than silver ink counterparts. Graphene and other carbon-based filaments are orders of magnitude less conductive than commercially available conductive pastes (~$10^{-5}$ Ω cm, $10^5$ S/cm). Even a filament comprised of copper-silver nanowire was only able to achieve resistivity values of 0.002 Ω cm (500 S/cm).[44] In electronics, because high resistance traces generate heat due to ohmic heating, choosing a material with the highest conductivity would be the best. Therefore, for the shell, a conductive paste will be used.

As mentioned previously in terms of conductive pastes, silver pastes are the preferred option because of their reliability, ease of use, and mild curing conditions which tend to be compatible with plastics. Copper conductive pastes have been demonstrated in the literature, however, require elevated temperatures and or toxic formate salts. Additionally, copper also oxidizes under ambient conditions further limiting its application. Silver thus will be used for the experiments.

The silver conductive paste used that has been used previously in this lab. It is has a conductivity on the order of $10^4$ S/cm when cured. It was prepared as described in the literature.[68] In brief, 0.4 g of TPU was dissolved in 2 g of anhydrous *N,N*-Dimethylformamide (DMF). To that, a suspension of silver nanoparticles (0.2 g) in 4 g of tetrahydrofuran (THF) was added and mixed briefly in a FlackTek SpeedMixer (1500 rpm, 5 min). To that mixture, 2 g of silver flake (2-5 µm, Inframat Advanced Materials, US) was added. The paste was mixed at 1500 rpm in the planetary mixture until a constant weight was achieved to ensure homogeneity. Silver paste was used as-is and stored at 4 °C when not in use.

### 3.2.3. Core Material Selection

For structural electronics and printed circuit boards (PCBs), a sturdy and heat-resistant material is desired and, in many cases, required. However, most plastics available for FFF 3D printing are unable to meet these requirements. One material that could work would be carbon fibre-reinforced (CFR) polylactic acid (PLA), and it has been shown to function well as a structural and insulating material.[30] Ideally, a CFR plastic would be used as these have some of the highest strengths available for commercial 3D printers.

Initial attempts with core-shell printing revealed an incompatibility with the paste and thermoplastic. Commonly available thermoplastics for 3D printing generally require temperatures in the range of 180 – 250 °C for printing. This high-temperature range excludes the use of all paste formulations as pastes contain volatile solvents which boil much below this temperature range. This results in premature curing of the paste within the nozzle itself, and or, could result in an explosion of the nozzle if sufficiently pressurized. A higher boiling point solvent, propylene carbonate (b.p. 242 °C), was also used as the solvent for the paste. However, pastes made with propylene carbonate also quickly evaporated in the nozzle and resulted in clogging. Even higher boiling point solvents, such as long-chain polyols, were considered but were not pursued as these would compromise the conductivity of the final paste. Impurities, such as the solvents, need to be fully removed to ensure a final conductive trace. Using a high-boiling solvent would be difficult to remove fully and would result in a loss of conductivity.

Instead of increasing the boiling point of the solvent, a lower melting thermoplastic was chosen as the core material.

### 3.2.4. Core Material Selection

As mentioned in 3.2.3, the thermal range from the paste precluded the use of the most common thermoplastics. The only suitable, commercially available filament was found to be Polycaprolactone (PCL).

PCL is a low melting thermoplastic with a printing range of 70 – 120 °C. It was found that a 70 – 80 °C printing range resulted in adequate print quality for both the thermoplastic and paste.

### 3.2.5. Magnetic Filament Preparation

Because the magnetic permeability of the surrounding material influences an inductor's properties, a magnetic filament was also prepared.

Polycaprolactone filament (PCL) was combined with Mn-ferrite powder (1-10 µM, Powertech International Corp.) for the preparation of this filament. To prepare Ferrite-PCL (20 wt%), PCL (Polymorph) was dissolved in an excess of THF. To that solution, a suspension of ferrite particles in THF was added and everything was mixed using a SpeedMixer at 1500 rpm for 5 min. The solution was then concentrated gradually under ambient conditions with mixing every 5-minutes. Once the suspension was highly viscous, it was dried under vacuum at 60 °C for 16 hours and processed into small grains (~4mm $^2$). The grains were then processed in a filament extruder (EX 6, Filabot, Ltd.) to prepare the composite filament for 3D printing. The extruder was heated to 79.6 °C, 78.0 °C, and 59.9 °C for the front, middle, and rear barrels respectively, and the material was processed at 15 rpm (Figure 3.3).

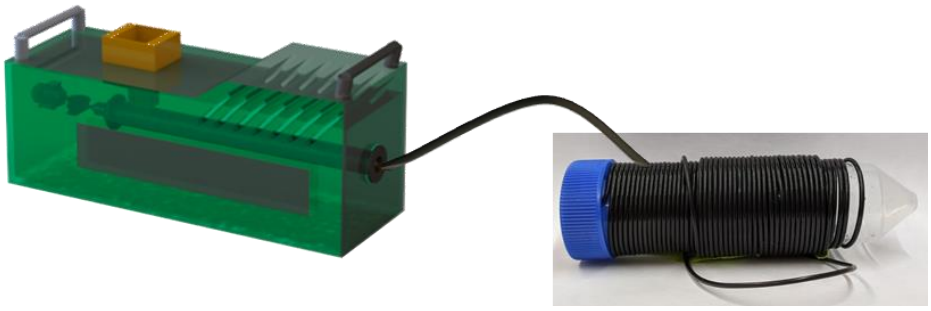

**Figure 3.3: Preparation of magnetic filament for core-shell 3D printing. The Filabot was used to extrude filament for printing.**

The magnetic permeability of the filament was determined using the Agilent E490A Precision LCR. Small sections of filament were tightly wrapped with copper transformer wire a known number of times. Based on the inductance of the fabricated inductor, equations 6 and 7 were used to calculate the relative permeability ($\mu_r$). N is the number of turns, μ is the magnetic permeability of the core, A is the cross-sectional area of the inductor, and L is the average length of the coil in meters. The magnetic permeability of the filament was determined to be 1.7 and the standard PCL filament had one of 1.3 based on five inductors.

$$L = \frac{N^2 \mu A}{L} \tag{3.1}$$

$$\mu = \mu_0 \mu_r \tag{3.1}$$

## 3.3. Core-Shell Inductors

For the inductance simulations, Ansys ® Electromagnetic Suite (2020 R1) was used. For single-point data, the magnetostatic solver was used with default settings. For frequency simulations, the eddy current solver was used with default settings. In all cases, an excitation current of 0.1 A was applied. Printing was conducted as described in section 3.3.4. Inductance measurements were conducted using the Agilent E490A Precision. Measurements were conducted using the LS-Q between 20 Hz and 2 MHz with four measurements for each data point. Prior to measurements, a background reading was taken to calibrate the instrument. The machine was also verified against a commercial inductor after calibration.

### 3.3.1. Preliminary Simulation of Core-Shell Inductors

To verify that changing the core material would not influence the inductance of the core-shell inductors, simulations were done with various core materials (figure 3.4) and a silver shell. Three core materials were considered: silver, dielectric ($\mu_r$ = 1), and magnetic ($\mu_r$ = 1000).

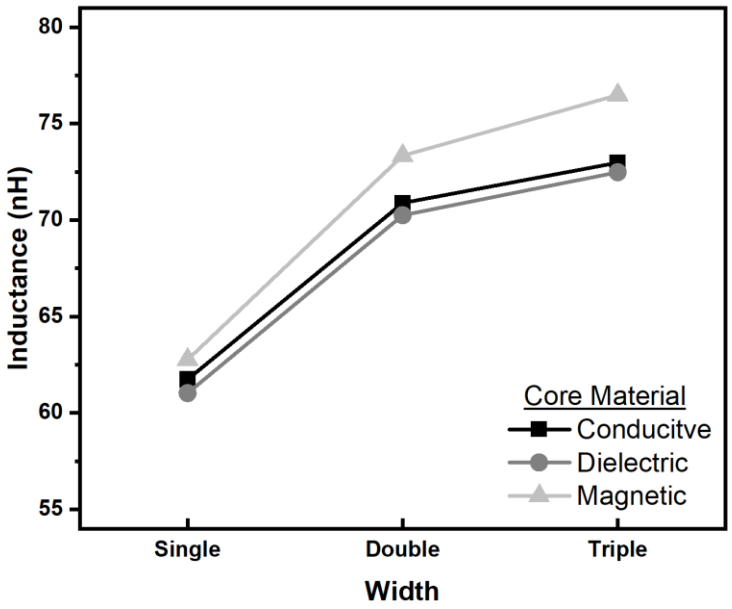


**Figure 3.4: Simulated inductance of single, double, and triple width inductors with various core materials.**

As expected, replacing the core material with a non-conductive material (dielectric) results in little change in the overall inductance across all three widths. The introduction of a magnetic core does result in an increase in the inductance with the effect more prominent at increased widths. It would be reasoned that a magnetic core would be more effective at a higher turn number as the magnetic core in one turn would act on the adjacent turn. This behaviour would be like coiling wire around a magnetic core to enhance inductance. An exploration of applications of a magnetic core would be interesting and is suggested for further exploration.

Overall, there is also an increased inductance when going from a single-width inductor to a triple-width inductor. The smaller increase between a double and a triple inductor could be attributed to the interplay between conductor width and inductor diameter. The increased diameter going from double to triple increases the inductance, but the increasing width is also known to cause a decrease in inductance.[55]

### 3.3.2. Simulation and Characterization of Core-Shell Inductors

Once it was confirmed by simulation that the use of a core-shell structure would not negatively impact the printed inductors, printing was conducted. Figure 3.5 shows the

printing of the single-width, double-width, and triple-width inductors. The printing was reasonably accurate and fully embedded inductors were printed.


**Figure 3.5: Prints of the single, double, and triple width inductors on PCL substrate.**

Fully embedded inductors were printed as previously described on either PCL or Ferrite-PCL (Fer). A subsequent layer of PCL was added after printing the conductive trace to embed the inductor. Finally, conductive traces were printed on the top to complete the circuit. A schematic representation is shown in Figure 3.6a. Figure 3.6b shows an exploded view of the embedded inductor. Figure 3.6 shows the for the single width inductor on PCL (Figure 6.6c) and on Fer (Figure 3.6d).

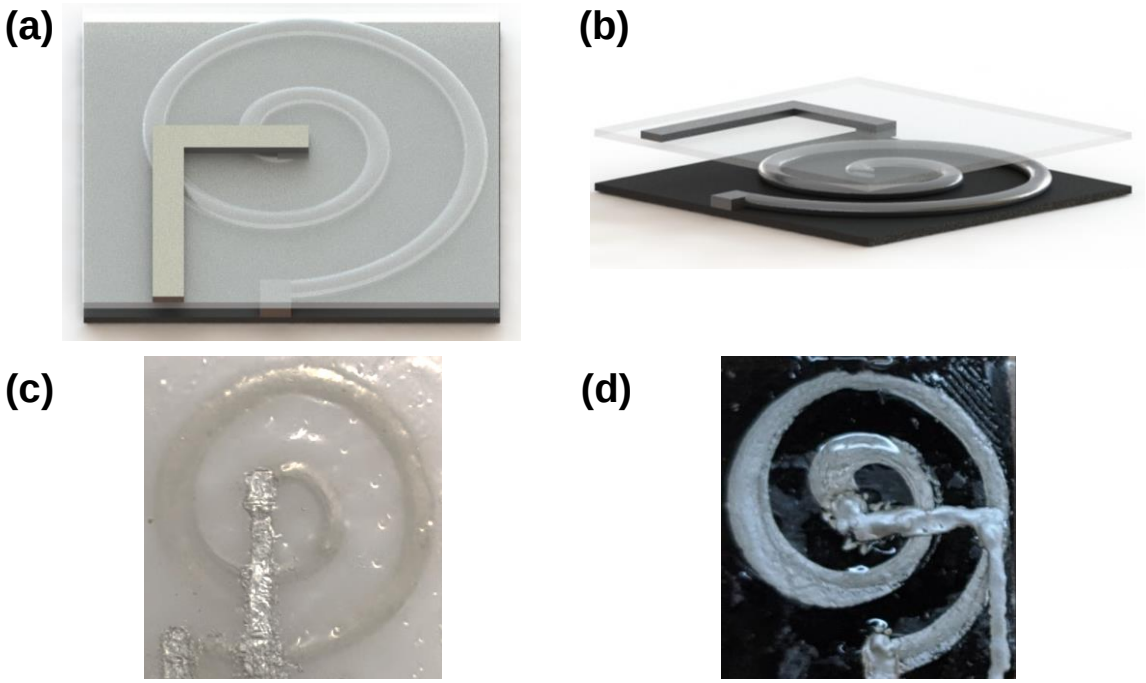


**Figure 3.6: CAD representation of single-width embedded inductors (a) and exploded view in (b). Printed samples with a backplane of PCL (c) and Ferrite-PCL (b).**

The simulated and experimental inductances for these inductors are shown in figure 3.7. Overall, the simulation and experimental results did show a trend of increasing inductance going from single to triple width inductors. Additionally, there was a difference observed when transitioning from PCL ($\mu_r$ ~1.3) to the Fer ($\mu_r$ ~ 1.7) backplane, despite the small increase in permeability. The difference was more obvious in the lower frequencies range (< 0.5 MHz) than at higher frequencies, but the presence of the backplane did result in a slight increase in inductance.

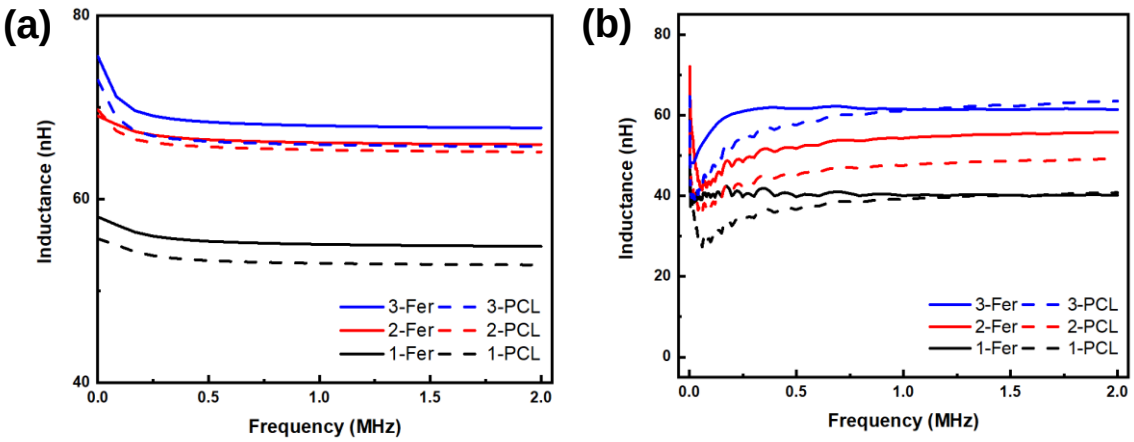


**Figure 3.7: Simulated and experimental inductances for embedded single, double, and triple width inductors printed on PCL and Ferrite-PCL (Fer) backplanes.**

Future research could be done to further enhance the magnetic properties of the filament by increasing the loading. In this experiment, a loading of 20% of ferrite was used as it showed reliable printability. However, it could be reasoned that a higher loading would be printable if optimized. Many commercial filaments have filler loading reaching approximately 40%.

# Chapter 4.

# Demonstration of Wireless Power Transfer with 3D Printed Inductors

## 4.1. Experimental Setup

The coupling coefficient and maximum power transfer efficiency are inductor specific. As discussed in section 1.5.3, the coupling coefficient in wireless power transfer (WPT) is dependent on the amount of flux between the receiving and transmitting coils. Factors that affect the amount of magnetic flux passing through the receiving coil affect the coupling coefficient and in turn the maximum power transfer efficiency. Distance, size mismatch, and presence of a magnetic backplane are all important factors in the coupling coefficient, and thus transfer efficiency. The quality factor of both the receiving and transmitting coil plays a significant role in the transfer efficiency only.

For the following measurements, coupling factor and maximum power transfer efficiency were determined with respect to a commercial transmitting coil (WT303012-12F2-ID, TDK Corporation) of comparable size and similar shape. Measurements were conducted using the Agilent E490A Precision. The instrument was set to the LS-Q mode and scans were conducted between 20 Hz and 2 MHz with four measurements for each data point. Prior to measurements, a background reading was taken to calibrate the instrument. The machine and procedure verified against a series of known commercial inductors after calibration and before sample measurement. Additionally, a two-turn coil of copper wire of similar size and shape to the printed inductors was also used. Inductances of such an inductor were in line with calculations. Thus, measurements of printed inductors were concluded to be reasonably accurate.

The coupling coefficient was calculated using equation 4.1. This measurement is conducted with the two coils in proximity (figure 4.1). $L_s$ is the measured inductance across $L_1$ with $L_2$ shorted. $L_o$ is the inductance of $L_1$ with $L_2$ left open. Based on the change in inductance, the coupling coefficient can be determined.

The maximum power transfer efficiency ($\eta_{max}$) is derived from the coupling coefficient (k) and the quality factor (Q) using equation 4.2. The LCR used for measurements also reports a quality factor reading and thus this was used for calculations.

$$k = \sqrt{\left(1 - \frac{L_s}{L_o}\right)} \tag{4.1}$$

$$\eta_{max} = \frac{k^2 Q_1 Q_2}{(kQ_1 + k^2 + 1)(kQ_2 + 1)} \tag{4.2}$$

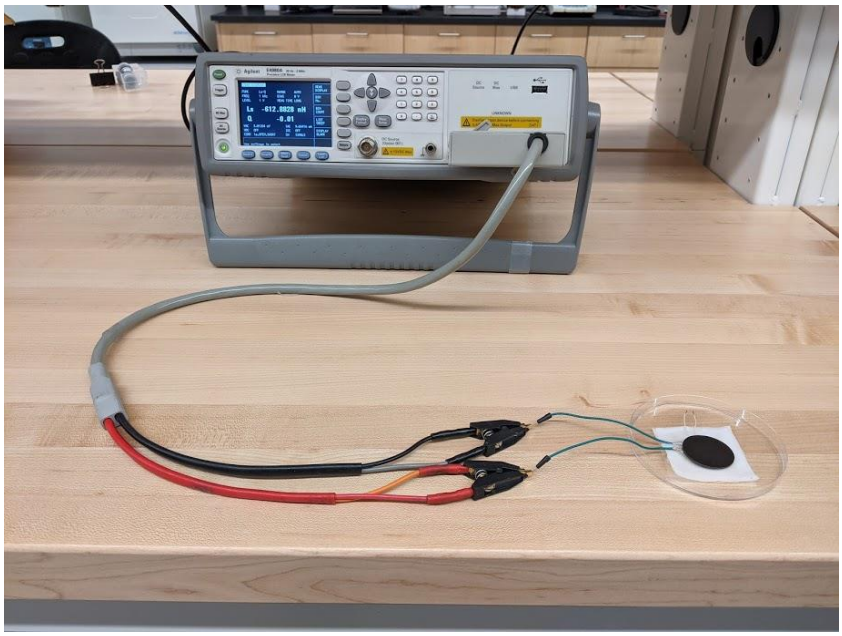

**Figure 4.1: Measurement of coupling coefficient using an LCR meter.**

Simulation of the coupling coefficient and maximum power transfer efficiency for the three printed inductors and the commercial inductor was conducted as described in section 3.3. Here, in brief, Ansys ® Electromagnetic Suite (2020 R1) was used to simulate the interaction between the two inductors. The eddy current solver was used in all cases with default settings.

## 4.2. Coupling Coefficient

The coupling coefficient is a measure of how well two coils are coupled. The results of the simulated and experimental are shown in figure 4.2. The simulation was conducted to provide an expectation of what the experimental results would look like. Further refinement of the model was not conducted as the experimental trend matched with the expected values.

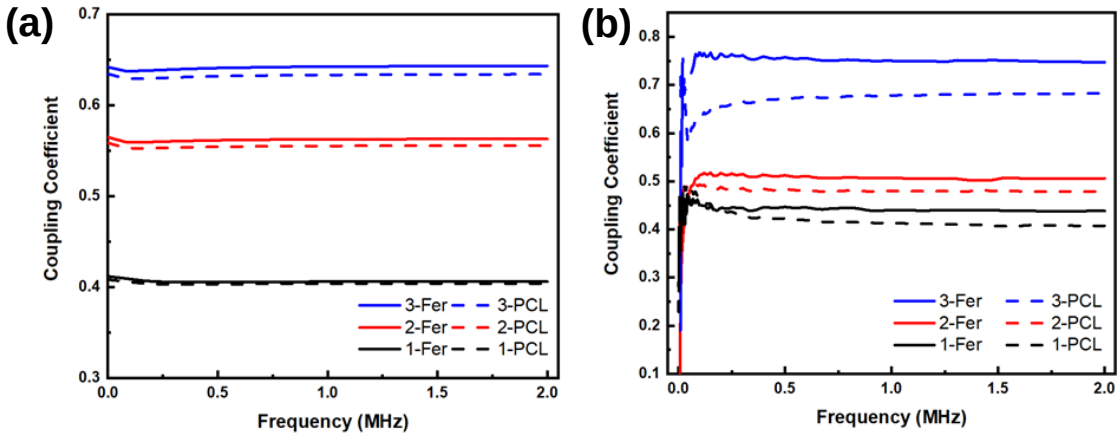


**Figure 4.2: Simulated (a) and experimental (b) results for coupling coefficient of single, double, and triple width inductors and commercial inductor.**

Overall, there is a trend of increasing coupling coefficient as the width increases from single to triple. This follows expectation as the commercial power transfer coil had dimensions most like the triple width inductor and least like the single width inductor. The coupling coefficient is dependent on the size of the two coupled inductors (section 1.7.3). In effect, the greater the overlap between the two coils, the greater the mutual inductance, and thus the greater the coupling coefficient as the coefficient is proportional to the square root of the mutual inductances (equation 1.5).

Another important factor in the coefficient is the separation between the transmitting and the receiving coil. For these experiments, the coils were placed as close as physically possible to ensure a consistent reading.

There was also an increase in coefficient observed in moving from a PCL backplane ($\mu_r$ ~ 1.3) to the more magnetic ferrite-PCL backplane ($\mu_r$ ~1.7). The change ranged from about 0.03 to 0.05, but it can be seen that small changes in permeability do induce significant

changes in the coupling coefficient. Comparable work has shown an increase of 0.13 in transitioning from no backplane (air, $\mu_r = 1$) to a slightly magnetic one ($\mu_r$ ~3).[62]

Overall, small changes do result in noticeable improvements in the coupling coefficient. As the materials available for 3D printing are being continually developed, more magnetic materials are becoming available for printing.[62], [69]–[72] As more magnetic materials become available, 3D printed electronics that rely on a magnetic material, such as the inductor shown here, will show increased performance.

## 4.3. Maximum Power Transfer Efficiency

In wireless power transfer systems, the coupling coefficient is not exactly the power transfer efficiency but is related to the efficiency (section 1.7.3). The results of the simulated and experimentally derived efficiencies are shown in figure 4.3. The simulation was to provide an expectation of the results and was not refined to be a complete match.

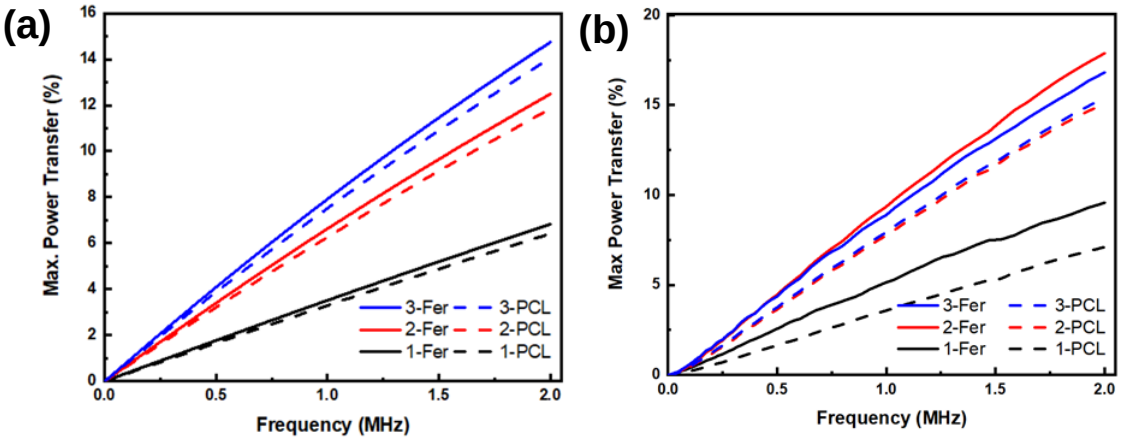


**Figure 4.3: Simulated (a) and experimental (b) results for the maximum power transfer efficiency single, double, and triple width inductors and commercial inductor.**

Overall, the addition of the magnetic backplane results in an increase in efficiency across both simulations and experimentally determined results. In addition, there is the expected trend of increased efficiency in moving from a single width to a triple width inductor is shown in the simulation. This same result is not seen experimentally. Instead, the double-width inductor seems to outperform or perform equally as well as the triple width inductor. An examination of the quality factor, and resistances, of the corresponding inductors,

suggest a possible explanation for the decrease in efficiency of the triple inductor. The double-width inductor has a higher quality factor than the triple-width inductor.

A possible reason for the observed differences could be the resistance readings of the respective inductors. Quality factor is proportional to inductance and inversely proportional to resistance (equation 1.8). In these inductors, the resistance seems to rise more quickly than the respective inductances, and this would result in the difference in quality factors observed.

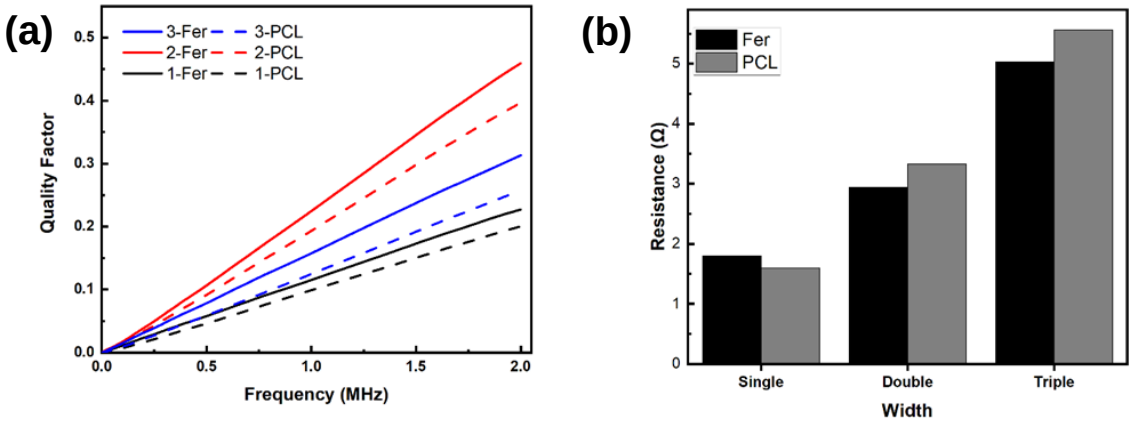


**Figure 4.4: Quality factor (a) and resistance measurements for the single, double, and triple width inductor.**

Improvements in the conductivity of pastes available for 3D printing would allow for better performing electronic components.

## 4.4. Conclusions

3D printed inductors were considered here for wireless power transfer. The printed inductors show a high coupling coefficient with the commercial power transfer coil with the triple width inductor showing the highest coupling coefficient. There is a lot of freedom in design and shape that can be realized due to the flexibility of 3D designs. Inductors with unique designs, as well as specific inductances, can be fabricated with the generated core-shell filament. Here, three different conductor widths and sizes were demonstrated, however, it would be possible to change the number of revolutions, the pattern, among other parameters. In this way, custom electronics can be produced while saving more material than otherwise would have been saved.

The addition of the 3D printed magnetic backplane adds the possibility of customization, but more critically, the inclusion allows for significant enhancements in the coupling coefficient of the inductors shown here; small changes in magnetic permeability of the backplane induce large changes in the properties of the inductor. Further work into generating more magnetic material for 3D printing would also result in further increases in these properties.

In addition to the coupling coefficient, the maximum power transfer efficiency is an important parameter in WPT applications. For these inductors, the maximum power transfer efficiency was relatively low compared to what could be attained through screen printing. However, this low efficiency originates from the poor-quality factor and high resistance of the inductors. The high resistance originates from the low conductivities accessible with currently available, and affordable printable materials. It can be reasoned as work continues to improve the conductivity of these paste that the efficiency would be increased.

For this work, a flexible plastic filament was used as core materials. For some applications this would be appropriate, however, the use of a high strength thermoplastic would be ideal in many other cases. Further developments into thermally stable pastes for 3D printing would allow for a wide range of selection for core materials. Thus, the core-shell printing shown here could be used to print inductive coils for applications that require much more reliable structures.

Overall, core-shell printed demonstrated here can be expanded to suit a wide variety of needs in many different settings.

# Chapter 5.

# Conclusions and Future Work

## 5.1. Conclusions

The transition to a more sustainable global society is an ongoing movement which requires greater sustainability at the economic, social, and environmental level. 3D printing will be an important contributor towards greater sustainability, especially regarding sustainable manufacturing. Because 3D printing is additive in nature, it allows for highly complex and customizable structures while also reducing material consumption and waste generation. Thus, 3D printing positions itself as a key technology in a more sustainable world.

One area of manufacturing that would benefit from the greater incorporation of 3D printing techniques would be the production of printed circuit boards and electronics. During the preparation of PCB, much of the initial copper that is deposited is etched away in subsequent steps, thus generating a lot of waste. However, because 3D printing is an additive technique, the conductive material is only deposited where it is desired, thereby limiting waste generation and material consumption. Additionally, with advances in multi-material 3D printing, it is possible to prepare structural electronics which further results in a reduction in material consumption.

In structural electronics, passive components, such as resistors, inductors, and capacitors, can be embedded within the structure of the electronic. Additionally, the substrate that electronic components sit in functions as part of the structure itself. Together, these two advances allow for an increased reduction in material consumption. However, there is further room for improvement, especially regarding the conductive traces used. 3D printed electronics require highly conductive material to function as traces, and this usually takes the form of a silver conductive paste. Carbon and copper-based materials do exist, however are either not as conductive or stable as silver pastes. Consequently, 3D-printed electronics on a large scale would be prohibitively expensive and unsustainable. Thus, it would be best to reduce the consumption of silver.

It is possible to reduce the amount of silver in a conductive trace by using a hollow or a sheath conductor. In this way, only a thin outer layer of a trace is conductive. In high-

alternating current applications, such as with inductive wireless power transfer, a hollow conductor in many cases would be better due to the skin effect.

With high frequency current, the current density in a conductor is localized to a thin layer at the surface of the conductor. This phenomenon is known as the skin effect. Overall, this reduces in higher effective resistance and greater ohmic losses. Thus, it is advantageous to utilize a hollow or a sheath conductor.

Coaxial printing was used to achieve the printing of these sheath conductors. The literature has several examples of coaxial extrusion for printing, but none in which a conductive material surrounds a core. Thus, this work presented an unexplored method of printing by coating a thermoplastic with a conductive metal paste. In this way, sheath conductors can be printed. To achieve this, several nozzles were designed and developed for printing.

The initial nozzle design showed poor heat distribution which resulted in poor printing quality. A subsequent design was prepared to be smaller and better at retaining heat. This design was successful during printing. In the effort to allow for greater customizability in nozzles, a similar experiment was conducted with plastic-based nozzles. These were unable to support the extrusion of thermoplastic, thus in further experiments, the second nozzle design in aluminum was used.

Using this nozzle inductors with various conductor widths were printed and tested for wireless power transfer. Simulations of the skin effect and the inductance measurements for core-shell printed inductors showed negligible differences between core-shell inductors and solid conductor inductors. Printed inductors indeed showed stable inductances and were projected to require less silver paste because the core of the conductive material was replaced with a thermoplastic. These inductors also showed good coupling with the commercial power transfer coil used in this study. The coil was chosen based on the inductors designed. The inclusion of a magnetic backplane was done and demonstrates the effectiveness that a slightly magnetic backplane has on increasing performance of inductors and suggests that more magnetic backplanes would further increase performance. These inductors, however, demonstrated poor power transfer efficiency. Because the conductivity of silver pastes is still lacking in comparison to bulk metal, the

inductors printed had relatively high resistances which lead to low quality factors and thus low power transfer efficiencies.

Overall, the work here illustrates the potential of using coaxial printing to reduce material consumption in the printing of structural electronics. The high customizability of 3D printing allows for unique structures fitted for any application. Wireless power transfer was demonstrated here, but many unique designs are possible. In addition, this work demonstrates a novel method of coaxial printing that combines paste printing with thermoplastic extrusion to generate sheath conductors.

## 5.2. Future Work

In this work, a planar spiral inductor was prepared and demonstrated. However, it would be possible to take the inductor into the third dimension and print high-performance 3D inductors. This would require optimization of the nozzle to allow for the quick switching between core printing and core-shell printing to build up dielectric material. Also, we can consider other core materials for structural electronics. The current work used a rather soft low melting polymer which is not suitable for long-lasting electronics. If instead a high-temperature resistant thermoplastic were used, the paste formulation would need to be modified, but it could work in the same way demonstrate. An alternative would be to switch to use a low-melting prepolymer which could be cross-linked after printing. In this way, the core could be printed, but later treated to be strong, rigid, and suitable for long-lasting electronics.

# References


[1] “Transforming our world: the 2030 Agenda for Sustainable Development | Department of Economic and Social Affairs.” [Online]. Available: https://sdgs.un.org/2030agenda. [Accessed: 03-Feb-2021].

[2] C. B. Joung, J. Carrell, P. Sarkar, and S. C. Feng, “Categorization of indicators for sustainable manufacturing,” *Ecol. Indic.*, vol. 24, pp. 148–157, Jan. 2013.

[3] H. T. Lee *et al.*, “Research Trends in Sustainable Manufacturing: A Review and Future Perspective based on Research Databases,” *International Journal of Precision Engineering and Manufacturing - Green Technology*, vol. 6, no. 4. Korean Society for Precision Engineering, pp. 809–819, 01-Aug-2019.

[4] S. H. Huang, P. Liu, A. Mokasdar, and L. Hou, “Additive manufacturing and its societal impact: A literature review,” *International Journal of Advanced Manufacturing Technology*, vol. 67, no. 5–8. Springer, pp. 1191–1203, 16-Jul-2013.

[5] M. Gebler, A. J. M. Schoot Uiterkamp, and C. Visser, “A global sustainability perspective on 3D printing technologies,” *Energy Policy*, vol. 74, no. C, pp. 158–167, Nov. 2014.

[6] C. Ihl and F. Piller, “3D Printing as Driver of Localized Manufacturing: Expected Benefits from Producer and Consumer Perspectives,” Springer, Cham, 2016, pp. 179–204.

[7] S. Ford and M. Despeisse, “Additive manufacturing and sustainability: an exploratory study of the advantages and challenges,” *J. Clean. Prod.*, vol. 137, pp. 1573–1587, Nov. 2016.

[8] M. K. Niaki, S. A. Torabi, and F. Nonino, “Why manufacturers adopt additive manufacturing technologies: The role of sustainability,” *J. Clean. Prod.*, vol. 222, pp. 381–392, Jun. 2019.

[9] B. P. Conner *et al.*, “Making sense of 3-D printing: Creating a map of additive manufacturing products and services,” *Addit. Manuf.*, vol. 1, pp. 64–76, Oct. 2014.

[10] N. Razaviarab, S. Sharifi, and Y. M. Banadaki, “Smart additive manufacturing empowered by a closed-loop machine learning algorithm,” no. March, p. 17, 2019.

[11] T. Kim, J. Vanloo, and W. S. Kim, “3D Origami Sensing Robots for Cooperative Healthcare Monitoring,” *Adv. Mater. Technol.*, p. 2000938, Jan. 2021.

[12] M. Kaur, T. G. Yun, S. M. Han, E. L. Thomas, and W. S. Kim, “3D printed stretching-dominated micro-trusses,” *Mater. Des.*, vol. 134, pp. 272–280, Nov. 2017.

[13] Y. Dong, C. Bao, and W. S. Kim, “Sustainable Additive Manufacturing of Printed Circuit Boards,” *Joule*, vol. 2, no. 4. Cell Press, pp. 579–582, 18-Apr-2018.

[14] R. Bansal, *Handbook of Engineering Electromagnetics*. Baton Rouge: CRC Press, 2004.

[15] P. D. Surya Santoso and H. W. Beaty, *Standard Handbook for Electrical Engineers, Seventeenth Edition*, 27th editi. New York: McGraw-Hill Education, 2018.

[16] W. H. (William H. Hayt, *Engineering electromagnetics / William H. Hayt, Jr., John A. Buck.*, 6th ed. McGraw-Hill, 2000.

[17] M. Rabia, H. Azzedine, and T. Lebey, “Modeling and dimensioning of a planar inductor for a monolithic integration,” in *Asia-Pacific Power and Energy Engineering Conference, APPEEC*, 2011.

[18] A. Kjar, B. McFarland, K. Mecham, N. Harward, and Y. Huang, “Engineering of tissue constructs using coaxial bioprinting,” *Bioact. Mater.*, vol. 6, no. 2, pp. 460–471, Feb. 2021.

[19] Q. Gao, Y. He, J. zhong Fu, A. Liu, and L. Ma, “Coaxial nozzle-assisted 3D bioprinting with built-in microchannels for nutrients delivery,” *Biomaterials*, vol. 61, pp. 203–215, Aug. 2015.

[20] X. Liu *et al.*, “Development of a Coaxial 3D Printing Platform for Biofabrication of Implantable Islet-Containing Constructs,” *Adv. Healthc. Mater.*, vol. 8, no. 7, p. 1801181, Apr. 2019.

[21] A. Adumitroaie, F. Antonov, A. Khaziev, A. Azarov, M. Golubev, and V. V. Vasiliev, “Novel continuous fiber bi-matrix composite 3-D printing technology,” *Materials (Basel).*, vol. 12, no. 18, Sep. 2019.

[22] F. Peng *et al.*, “3D Printing with Core–Shell Filaments Containing High or Low Density Polyethylene Shells,” *ACS Appl. Polym. Mater.*, vol. 1, no. 2, pp. 275–285, Feb. 2019.

[23] M. A. H. Khondoker, A. Ostashek, and D. Sameoto, “Direct 3D Printing of Stretchable Circuits via Liquid Metal Co-Extrusion Within Thermoplastic Filaments,” *Adv. Eng. Mater.*, vol. 21, no. 7, p. 1900060, Jul. 2019.

[24] B. Deore *et al.*, “Direct printing of functional 3D objects using polymerization-induced phase separation,” *Nat. Commun.*, vol. 12, no. 1, pp. 1–12, Dec. 2021.

[25] D. Espalin, D. W. Muse, E. MacDonald, and R. B. Wicker, “3D Printing multifunctionality: Structures with electronics,” *Int. J. Adv. Manuf. Technol.*, vol. 72, no. 5–8, pp. 963–978, Mar. 2014.

[26] A. D. Valentine *et al.*, “Hybrid 3D Printing of Soft Electronics,” *Adv. Mater.*, vol. 29, no. 40, Oct. 2017.

[27] D. J. Roach, C. M. Hamel, C. K. Dunn, M. V. Johnson, X. Kuang, and H. J. Qi, “The m4 3D printer: A multi-material multi-method additive manufacturing platform for future 3D printed structures,” *Addit. Manuf.*, vol. 29, p. 100819, Oct. 2019.

[28] E. MacDonald *et al.*, “3D printing for the rapid prototyping of structural electronics,” *IEEE Access*, vol. 2, pp. 234–242, 2014.

[29] B.-H. Lu, H.-B. Lan, and H.-Z. Liu, “Additive manufacturing frontier: 3D printing electronics,” *Opto-Electronic Adv.*, vol. 1, no. 1, pp. 17000401–17000410, Feb. 2018.

[30] S. Swaminathan, K. B. Ozutemiz, C. Majidi, and S. E. Hudson, “FiberWire: Embedding Electronic Function into 3D Printed Mechanically Strong, Lightweight Carbon Fiber Composite Objects,” *Proc. 2019 CHI Conf. Hum. Factors Comput. Syst. - CHI ’19*, no. Figure 1, pp. 1–11, 2019.

[31] Y. Dong, X. Min, and W. S. Kim, “A 3-D-Printed Integrated PCB-Based Electrochemical Sensor System,” *IEEE Sens. J.*, vol. 18, no. 7, pp. 2959–2966, Apr. 2018.

[32] M. Yu, X. Zeng, Q. Song, L. Liu, and J. Li, “Examining regeneration technologies for etching solutions: A critical analysis of the characteristics and potentials,” *Journal of Cleaner Production*, vol. 113. Elsevier Ltd, pp. 973–980, 01-Feb-2016.

[33] O. Cakir, “Copper etching with cupric chloride and regeneration of waste etchant,” *J. Mater. Process. Technol.*, vol. 175, no. 1–3, pp. 63–68, Jun. 2006.

[34] Z. Huang, F. Xie, and Y. Ma, “Ultrasonic recovery of copper and iron through the simultaneous utilization of Printed Circuit Boards (PCB) spent acid etching solution and PCB waste sludge,” *J. Hazard. Mater.*, vol. 185, no. 1, pp. 155–161, 2011.

[35] N. V. Mdlovu, C. L. Chiang, K. S. Lin, and R. C. Jeng, “Recycling copper nanoparticles from printed circuit board waste etchants via a microemulsion process,” *J. Clean. Prod.*, vol. 185, pp. 781–796, Jun. 2018.

[36] M. Kaur, T.-H. Kim, and W. S. Kim, “New Frontiers in 3D Structural Senesing Robots,” *Adv. Mater.*, p. 2002534, 2020.

[37] M. Ankenbrand, Y. Eiche, and J. Franke, “Programming and evaluation of a multi-Axis/multi-process manufacturing system for mechatronic integrated devices,” in *2019 International Conference on Electronics Packaging, ICEP 2019*, 2019, pp. 273–278.

[38] H. H. H. Maalderink *et al.*, “3D Printed structural electronics: embedding and connecting electronic components into freeform electronic devices,” *Plast. Rubber Compos.*, vol. 47, no. 1, pp. 35–41, Jan. 2018.

[39] C. Tröger, A. T. Bens, G. Bermes, R. Klemmer, J. Lenz, and S. Irsen, “Ageing of acrylate-based resins for stereolithography: Thermal and humidity ageing behaviour studies,” *Rapid Prototyp. J.*, vol. 14, no. 5, pp. 305–317, 2008.

[40] C. K. Chua, K. F. Leong, and C. S. Lim, *Rapid Prototyping: Principles and Applications*. WORLD SCIENTIFIC, 2003.

[41] S. W. Kwok *et al.*, “Electrically conductive filament for 3D-printed circuits and sensors,” *Appl. Mater. Today*, vol. 9, pp. 167–175, 2017.

[42] A. Dorigato, V. Moretti, S. Dul, S. H. Unterberger, and A. Pegoretti, “Electrically conductive nanocomposites for fused deposition modelling,” *Synth. Met.*, vol. 226, pp. 7–14, 2017.

[43] J. C. Tan and H. Y. Low, “Embedded electrical tracks in 3D printed objects by fused filament fabrication of highly conductive composites,” *Addit. Manuf.*, vol. 23, pp. 294–302, Oct. 2018.

[44] M. A. Cruz *et al.*, “Multigram Synthesis of Cu-Ag Core-Shell Nanowires Enables the Production of a Highly Conductive Polymer Filament for 3D Printing Electronics,” *Part. Part. Syst. Charact.*, vol. 35, no. 5, p. 1700385, May 2018.

[45] K. Andersen, Y. Dong, and W. S. Kim, “Highly Conductive Three-Dimensional Printing With Low-Melting Metal Alloy Filament,” *Adv. Eng. Mater.*, vol. 19, no. 11, p. 1700301, Nov. 2017.

[46] W. Li *et al.*, “The rise of conductive copper inks: challenges and perspectives,” *Applied Materials Today*, vol. 18. Elsevier Ltd, p. 100451, 01-Mar-2020.

[47] S. K. Tam, K. Y. Fung, and K. M. Ng, “Copper pastes using bimodal particles for flexible printed electronics,” *J. Mater. Sci.*, vol. 51, no. 4, pp. 1914–1922, Feb. 2016.

[48] M. Kanzaki, Y. Kawaguchi, and H. Kawasaki, “Fabrication of Conductive Copper Films on Flexible Polymer Substrates by Low-Temperature Sintering of Composite Cu Ink in Air,” *ACS Appl. Mater. Interfaces*, vol. 9, no. 24, pp. 20852–20858, Jun. 2017.

[49] Y. Li, T. Qi, M. Chen, and F. Xiao, “Mixed ink of copper nanoparticles and copper formate complex with low sintering temperatures,” *J. Mater. Sci. Mater. Electron.*, vol. 27, no. 11, pp. 11432–11438, Nov. 2016.

[50] J. Borremans, P. Wambacq, C. Soens, Y. Rolain, and M. Kuijk, “Low-area active-feedback low-noise amplifier design in scaled digital CMOS,” *IEEE J. Solid-State Circuits*, vol. 43, no. 11, pp. 2422–2433, Nov. 2008.

[51] P. F. Flowers, C. Reyes, S. Ye, M. J. Kim, and B. J. Wiley, “3D printing electronic components and circuits with conductive thermoplastic filament,” *Addit. Manuf.*, vol. 18, pp. 156–163, Dec. 2017.

[52] Y. Yan, J. Moss, K. D. T. Ngo, Y. Mei, and G. Q. Lu, “Additive manufacturing of toroid inductor for power electronics applications,” in *ECCE 2016 - IEEE Energy Conversion Congress and Exposition, Proceedings*, 2016.

[53] Y. He *et al.*, “Three-Dimensional Coprinting of Liquid Metals for Directly Fabricating Stretchable Electronics,” *3D Print. Addit. Manuf.*, vol. 5, no. 3, pp. 195–203, Sep. 2018.

[54] J. R. Jian, T. Kim, J. S. Park, J. Wang, and W. S. Kim, “High performance 3D printed electronics using electroless plated copper,” *AIP Adv.*, vol. 7, no. 3, p. 035314, Mar. 2017.

[55] S. Stalf, “Printed inductors in RF consumer applications,” *IEEE Trans. Consum. Electron.*, vol. 47, no. 3, pp. 426–435, Aug. 2001.

[56] M. McDonough and B. Fahimi, “Comparison between circular and square coils for use in Wireless Power Transmission,” in *IET Conference Publications*, 2014, vol. 2014, no. 627 CP.

[57] H. Jiang *et al.*, “A low-frequency versatile wireless power transfer technology for biomedical implants,” *IEEE Trans. Biomed. Circuits Syst.*, vol. 7, no. 4, pp. 526–535, 2013.

[58] T. Sun, X. Xie, and Z. Wang, *Wireless power transfer for medical microsystems*, vol. 9781461477. New York, NY: Springer New York, 2013.

[59] H. Lakhal, M. Dhieb, H. Ghariani, and M. Lahiani, “Wireless power transmission technologies and applications,” in *14th International Conference on Sciences and Techniques of Automatic Control and Computer Engineering, STA 2013*, 2013, pp. 168–173.

[60] G. A. Covic and J. T. Boys, “Inductive power transfer,” *Proc. IEEE*, vol. 101, no. 6, pp. 1276–1289, 2013.

[61] T. Sun, X. Xie, and Z. Wang, *Wireless Power Transfer for Medical Microsystems*. New York, NY: Springer New York, 2013.

[62] N. Lazarus and S. S. Bedair, “Improved power transfer to wearable systems through stretchable magnetic composites,” *Appl. Phys. A Mater. Sci. Process.*, vol. 122, no. 5, pp. 1–7, May 2016.

[63] N. Lazarus, S. S. Bedair, and G. L. Smith, “Creating 3D printed magnetic devices with ferrofluids and liquid metals,” *Addit. Manuf.*, vol. 26, pp. 15–21, Mar. 2019.

[64] J. Kim *et al.*, “Coil design and shielding methods for a magnetic resonant wireless power transfer system,” *Proc. IEEE*, vol. 101, no. 6, pp. 1332–1342, 2013.

[65] “Magnetic Resonance and Magnetic Induction What is the best choice for my application?” .

[66] S. Han and D. D. Wentzloff, “Wireless power transfer using resonant inductive coupling for 3D integrated ICs,” in *IEEE 3D System Integration Conference 2010, 3DIC 2010*, 2010.

[67] “Product - CERES Print System | Exaddon AG.” [Online]. Available: https://www.exaddon.com/product. [Accessed: 11-Feb-2021].

[68] C. Bao, M. Kaur, and W. S. Kim, “Toward a highly selective artificial saliva sensor using printed hybrid field effect transistors,” *Sensors Actuators, B Chem.*, vol. 285, pp. 186–192, Apr. 2019.

[69] E. Dohmen, A. Saloum, and J. Abel, “Field-structured magnetic elastomers based on thermoplastic polyurethane for fused filament fabrication,” *Philos. Trans. R. Soc. A Math. Phys. Eng. Sci.*, vol. 378, no. 2171, May 2020.

[70] L. M. Bollig, P. J. Hilpisch, G. S. Mowry, and B. B. Nelson-Cheeseman, “3D printed magnetic polymer composite transformers,” *J. Magn. Magn. Mater.*, vol. 442, pp. 97–101, Nov. 2017.

[71] Y. Arbaoui *et al.*, “3D printed ferromagnetic composites for microwave applications,” *J. Mater. Sci.*, vol. 52, no. 9, pp. 4988–4996, May 2017.

[72] M. Ralchev, V. Mateev, and I. Marinova, “3D Printing of Magnetic Materials by FFF Technology,” 2021, pp. 1–4.